Biochemical and Biophysical Research Communications 772 (2025) 152053

Contents lists available at ScienceDirect

Biochemical and Biophysical Research Communications

journal homepage: www.elsevier.com/locate/ybbrc

Characterization and comparison of two NPC cell lines, C17 and C666-1, as models for studying the pathogenesis of nasopharyngeal carcinoma

Anna Makowska [a,*], Eva Miriam Buhl [b], Maximilian Göschel [a], Chao-Chung Kuo [c], Christina Nothbaum [a], Emel Aylin Toktamis [a], Lian Shen [a], Ali T. Abdallah [d,e], Ralf Weiskirchen [f], Udo Kontny [a]

[a] Division of Pediatric Hematology, Oncology and Stem Cell Transplantation, University Hospital Aachen, D-52074, Aachen, Germany
[b] Electron Microscopy Facility, Institute of Pathology, University Hospital Aachen, D-52074, Aachen, Germany
[c] Genomics Facility, Interdisciplinary Center for Clinical Research (IZKF), RWTH Aachen University, Aachen, Germany
[d] Cluster of Excellence Cellular Stress Responses in Aging-Associated Diseases (CECAD), Medical Faculty and University Hospital Cologne, University of Cologne, D-50931, Cologne, Germany
[e] Institute of Medical Statistics and Computational Biology, Faculty of Medicine, University of Cologne, D-50924, Cologne, Germany
[f] Institute of Molecular Pathobiochemistry, Experimental Gene Therapy and Clinical Chemistry (IFMPEGKC), University Hospital Aachen, D-52074, Aachen, Germany

ARTICLE INFO

Keywords:
Nasopharyngeal carcinoma (NPC)
Epstein-barr virus
Cancer
Cell lines
Cell culture
Cell characterization
International cell line authentication committee (ICLAC)

ABSTRACT

Nasopharyngeal carcinoma (NPC) is a malignant tumor that originates from the epithelial cells of the nasopharynx. NPC is closely linked to Epstein-Barr virus (EBV) infection, which necessitates the use of EBV-positive cell lines for accurate pathology studies. In this paper, we present a detailed comparison of the C666–1 and C17 cell lines using bulk RNA-sequencing (RNA-Seq) methods. By thoroughly examining the gene expression profiles of these cell lines, we aim to elucidate the molecular mechanisms that drive NPC progression and metastasis. Understanding these mechanisms is crucial for developing effective treatment strategies. Cancer cell line models are essential in this research, as they provide a controlled environment for studying the complex interplay between viral and host cellular factors. Additionally, our study highlights the differences between the two cell lines, which could be pivotal in designing new experiments and tailoring therapeutic approaches.

1. Introduction

Nasopharyngeal carcinoma (NPC) is a type of tumor that originates from the epithelial cells of the nasopharynx. It has the highest incidence rates in Southern China, with significantly lower rates in Europe and the Americas [1–4]. Most NPC patients are diagnosed at advanced stages, often with cervical lymph node metastasis [5]. The exact cause of NPC remains unclear, but various risk factors have been identified, including genetic variations, viral infections, and environmental factors [6–8]. NPC is highly malignant and prone to metastasis, making treatment and management challenging. The standard treatment for advanced NPC involves a combination of radiotherapy and chemotherapy, resulting in cure rates of 80 %–90 % for patients without distant metastases. Radiotherapy, while effective, can result in substantial immediate and long-term side effects, including painful inflammation of the mucous membranes (mucositis), persistent dry mouth (xerostomia), and loss of hearing [9–11].

NPC is closely linked to Epstein-Barr virus (EBV) infection, requiring the use of EBV-positive cell lines for accurate pathology studies [12,13]. EBV, a Group I carcinogen, is involved in 95 % of NPC cases in endemic regions and 20 % in areas with lower incidence [14]. However, the presence of EBV in NPC tumor tissue is not universal. Several factors contribute to this variability, such as geographic regions, ethnic groups and environmental factors [14]. Histologically, a non-keratinizing NPC subtype is associated with EBV, a keratinizing subtype is linked to smoking, and a very rare basaloid subtype [15].

Circulating EBV DNA strongly correlates with tumor burden and serves as a robust prognostic biomarker in NPC [16–18]. High levels of EBV DNA in blood indicate more aggressive tumors and poorer survival outcomes [18]. EBV DNA status remains a significant independent

* Corresponding author.
E-mail addresses: amakowska@ukaachen.de (A. Makowska), ebuhl@ukaachen.de (E.M. Buhl), magoeschel@ukaachen.de (M. Göschel), ckuo@ukaachen.de (C.-C. Kuo), christina.nothbaum@rwth-aachen.de (C. Nothbaum), emtoktamis@ukaachen.de (E.A. Toktamis), lshen@ukaachen.de (L. Shen), ali.abdallah@gmail.com (A.T. Abdallah), rweiskirchen@ukaachen.de (R. Weiskirchen), ukontny@ukaachen.de (U. Kontny).

https://doi.org/10.1016/j.bbrc.2025.152053
Received 14 March 2025; Received in revised form 14 May 2025; Accepted 19 May 2025
Available online 20 May 2025

prognostic factor, influencing medical studies, clinical trials, and treatment plans. The TNM (Tumor, Node, Metastasis) classification system uses EBV DNA levels to correlate with tumor burden and metastasis, often associating high levels with advanced stages and extensive spread [19,20]. EBV expresses latent proteins such as *EBNA1* and *LMP1*, which can interact with cellular pathways to promote oncogenesis. For example, *LMP1* can mimic a constitutively active receptor, leading to uncontrolled cell growth [21]. EBV can induce epigenetic changes in the host genome, such as DNA methylation and histone modification, which can lead to the activation of oncogenes and the silencing of tumor suppressor genes [14]. EBV helps infected cells evade an immune response, enabling them to proliferate uncontrollably [21].

EBV-positive cell lines are crucial for studying NPC because NPC is closely associated with EBV infection. These cell lines help researchers understand how EBV contributes to the development and progression of NPC and are used to test potential treatments. However, several previously published NPC cell lines have lost their episomal EBV after prolonged culture. The 13th version of the International Cell Line Authentication Committee (ICLAC) lists 21 NPC cell lines as initially EBV-positive, but many of these have lost their EBV status over time. Among the few EBV-positive NPC cell lines that have retained their status are C17 and C666-1 [22].

Due to the significance of EBV for NPC pathogenesis, research on NPC has mainly focused on EBV-related proteins and genes, such as the EBV-encoded RNA EBER and the EBV-associated membrane antigen LMP [12,23]. In this paper, we present a detailed comparison of the C666–1 and C17 cell lines using bulk RNA-sequencing (RNA-Seq) method. This method allows for a comprehensive analysis of genetic and epigenetic changes, providing insights into the molecular underpinnings of NPC.

2. Materials and methods

2.1. Literature search

Papers that worked with C666–1 and C17 cells were identified by searching various databases such as PubMed, PMC, Web of Science, and Medline on October 1, 2024. The search terms used were “C666-1” or “C17” and “nasopharyngeal carcinoma” or “nasopharyngeal neoplasm”.

2.2. Reagents

SuperScript III Reverse Transcriptase was obtained from Invitrogen-Thermo Fisher Scientific (Darmstadt, Germany; #18080044). The RNeasy Mini Kit was purchased from Qiagen (Hilden, Germany; #74104). The NextSeq 500/550 High Output Kit v2.5 (150 cycles) was obtained from Illumina (San Diego, USA; #20024907). The RNA ScreenTape Assay was purchased from Agilent Technologies (Santa Clara, California, USA; #5067–5576) and the Ribo-Zero Gold Kit was obtained from Illumina (#RS-122-2301). The TruSeq® Stranded Total RNA Library Preparation Kit was purchased from Illumina (#20020596) and the D1000 ScreenTape Assay was obtained from Agilent Technologies (Santa Clara, California, USA; #5067–5582). The Maxwell® RSC simplyRNA Tissue Kit was purchased from Promega (Madison, Wisconsin, USA; #AS1340). The primers used in this study were obtained from Eurofins Genomics (Ebersberg, Germany). Monoclonal antibodies: APC-*anti*-human EpCam (#324208), PE-*anti*-human EGFR (#352904), PE-*anti*-human ICAM1 (#353106), PE-*anti*-human ERBB2 (#334406), PE-*anti*-human B7H3 (#331606), APC-mouse IgG2b (#401210), PE-mouse IgG1k (#400112), APC- anti-human CD80 (#30522), APC-anti-human CD86 (#305412), APC- anti-human Nectin-2 (#337412), APC- anti-human Galectin-9 (#348908), APC- anti-human PVR (#337618), APC- anti-human HLA-A (#343308), APC- anti-human HLA-E (#342606), HLA-DR (#327022), CEACAM-1 (#342304) were obtained from BioLegend (San Diego, California, USA).

2.3. Cell lines, culture condition and EBV status

In this study, NPC cell lines HK1, C666-1, and C17 were used. The HK1 cell line was obtained from Prof. Kwok Wai Lo at the Chinese University of Hong Kong, China. This cell line was cultured in DMEM medium (Gibco, Paisley, UK) supplemented with 10 % fetal bovine serum (Gibco) and 100 U/mL penicillin and 100 mg/mL streptomycin (Gibco). The C666-1 cell line was provided by Prof. Fei-Fei Liu from the University of Toronto, Canada [13], while the C17 cell line was obtained from Prof. Sai Wah Tsao at the Chinese University of Hong Kong, China [23]. Both cell lines were cultured in RPMI1640 medium (Gibco) supplemented with 10 % fetal bovine serum (Gibco) and 100 U/mL penicillin and 100 mg/mL streptomycin (Gibco). Additionally, the RPMI1640 medium for the C17 cell line included the Rho-associated coiled-coil containing kinases inhibitor (Y-76 27632) (#S1049, Selleckchem, Munich, Germany). The cells were grown in a humidified incubator with 95 % air and 5 % CO_2 at 37 °C. EBV detection in cell culture supernatants of C666–1 and C17 cells was conducted using the copy number assay as previously described in detail [24].

2.4. Quantification of NPC cell line growth

Both NPC cell lines, C666–1 and C17, were seeded in 12-well plates with an initial seeding number of 4 x 10^4 cells per well. Triplicates were then trypsinized, stained with 0.2 % trypan blue, and counted. The average cell number was calculated and this process was repeated every 24 h until the cells nearly ceased proliferation. This allowed for the determination of growth curves and the precise growth properties of NPC in culture. The number of cell doublings was calculated using the formula:

$$\text{Doubling Time} = [\mathrm{T} \times (\ln 2)] \div [ln(Y|X)]$$

Where T represents the time, X represents the cell number at the start, and Y represents the number of cells at the end.

2.5. Cell imaging

Both NPC cell lines, C666–1 and C17, were cultured in cell culture flasks that had been treated with vacuum gas plasma to ensure consistent cell attachment and growth. These flasks were made from crystal-clear virgin polystyrene, were sterile and certified non-pyrogenic (#734–2313; VWR, Radnor, PA USA). The cells were observed under a light microscope at 100x, 200x and 400× magnifications.

2.6. Short tandem repeat profiling

To address the significant problem of HeLa contamination in NPC research, we conducted confirmation through STR profiling [25]. The STR profiling and tests for interspecies contamination of the various cell lines used in this study were conducted using the cell line authentication service provided by IDEXX BioAnalytics (Kornwestheim, Germany). They employed the CellCheck™ Human system, which includes 16 species-specific STR markers. Eight of these markers are based on guidelines from the American Tissue Culture Collection (ATCC), which recommends a minimum of eight core STR loci (CSF1PO, D13S317, D16S539, D5S818, D7S820, TH01, TPOX, and vWA), as well as the Amelogenin (AMEL) gene for gender determination [26–28]. Additionally, the CellCheck™ Human system includes seven additional markers (D18S51, D21S11, D3S1358, D8S1179, FGA, Penta D, and Penta E), which enhances the robustness of the analysis.

2.7. Electron microscopy

Cell platelets were fixed in 3 % glutaraldehyde in 0.1 M Soerensen’s phosphate buffer (Merck, Darmstadt, Germany) for 24h and embedded

in 2.5 % low-melting agarose (Sigma, Steinheim, Germany). After post-fixing with 1 % OsO4 (Roth, Karlsruhe, Germany) in 25 mM sucrose buffer (Merck, Darmstadt, Germany) the samples were dehydrated using an ascending ethanol series (30 %, 50 %, 70 %, 90 % and 100 %) for 10 min each. This dehydration process was repeated three times. The dehydrated samples were then incubated in a mixture of Epon resin (Serva, Heidelberg, Germany) and ethanol (1:1) for 1h, followed by pure Epon for an additional hour. The samples were embedded in fresh Epon and polymerized at 90 °C for 2h. Ultrathin sections (90 nm) were stained with 0.5 % uranyl acetate and 1 % lead citrate (both EMS, Munich, Germany) to enhance contrast. The samples were examined using a transmission electron microscope (Zeiss Leo906, Oberkochen, Germany) operating at an acceleration voltage of 60 kV.

2.8. RNA extraction, library construction and next generation sequencing

Total RNA was isolated from NPC cell lines C17 and C666-1. The Maxwell RSC Simply RNA Tissue kit from Promega was used following the manufacturer's instructions. RNA quality assessment was performed using the RNA screen tape assay on the Agilent 4200 Tape Station (Agilent), and quantification was carried out using the Quantus Fluorometer from Promega. Libraries were generated from 1 μg of total RNA using the TrueSeq Stranded Total RNA Library Prep Kit and the Ribo-Zero Gold Kit (both from Illumina), as specified by the manufacturer. The quality and quantity of the RNA libraries were evaluated using the D1000 screen tape assay on the 4200 Tape Station and the Quantus Fluorometer, respectively. Subsequently, the libraries were sequenced on an Illumina NextSeq 500 platform using the High Output 150 cycles Kit (2 × 76 cycles, paired-end reads, single index) (Illumina), resulting in an average of 101.5 million reads per sample. Samples were then processed using the publicly available nf-core/RNA-Seq pipeline version 3.12 [29] implemented in Nextflow 23.10.0 [30] with the minimal command. All analysis was performed using custom scripts in R version 4.3.3.

2.9. Quantitative real-time PCR

Total cellular RNA was extracted using the RNeasy Mini Kit (Qiagen). Complementary DNA was synthesized using the SuperScript III Reverse Transcriptase (Thermo Fisher Scientific) according to the manufacturer's protocol. Quantitative real-time PCR (RT-qPCR) was performed using 2x SYBR Green qPCR Master Mix (Bimake). The primers used in this study are listed in Table 1.

For analysis of the EBV gene expression profile, we implemented a two-step normalization process. Initially, we normalized the samples using β-actin as an internal reference gene to accurately determine the expression of the target gene relative to β-actin in each cell line. Subsequently, we compared the normalized expression levels of the target gene in the positive cell line with those in the negative cell line. This two-step normalization approach allowed us to more precisely quantify the differences between the cell lines and ensured that our results were both robust and reproducible.

2.10. Flow cytometry

The surface expression of *EpCAM*, *ICAM1*, *ERBB2*, *EGFR*, and *B7H3/CD276* on C666–1 and C17 cells was assessed using flow cytometry following the manufacturer's protocol. Initially, untreated NPC cells were suspended at a density of 1×10^6 cells in 500 μl of medium and then incubated with 5 μl of mouse anti-human antibodies for a minimum of 30 min on ice. Subsequently, the samples were rinsed in PBS and analyzed by flow cytometry. Data analysis was carried out using FlowJo software, and each assay was repeated in three independent experiments.

2.11. STR similarity search

All STR similarity searches were conducted using the Cellosaurus STR Similarity Search Tool, CLASTR 1.4.4 (release 41.0) [48]. Additional information about the Cellosaurus STR database can be found in other sources [49]. The specific search parameters for each query were

Table 1
Primer sequences used to validate selected DEGs.

Gene	Forward-Prime (5′-3′)	Reverse-Prime (5′-3′)	Reference
UCHL1	AGCTCAAGCCGATGGAGATC	CCCTTCAGCTCTTCAATCTG	[31]
GSTA3	GTCGCTATTTCCCTGCCTTCGA	GTTCCACCAGGCTAATGTCAGC	[32]
RET	GTCCTCTTGCTCCACTTCAACG	CCTGGCAGTTTTCCACACAGAC	[33]
FGFR1	GCACATCCAGTGGCTAAAGCAC	AGCACCTCCATCTCTTTGTCGG	[34]
EBNA1	GAGAAGGCCCAAGCACTG	CTCCTTGACCACGATGCTTT	[35]
EBNA2	TTTCACCAATACATGAACC	TGGCAAAGTGCTGAGAGCAA	[36]
EBER1/2	GAGGTTTTGCTAGGGAGGAGA	CACCACCCGGGACTTGTA	[35]
LMP1	GTCCTGTGGGCCATTGTC	CCCACTCTGCTCTCAAAACC	[35]
LMP2	GACATGAAGAGCACGAAGAGC	TTCTCATGCTCCTATGGACACTT	[35]
RPMS1	CCCAAGCTTCATGGCCGGAGCTCGTCGAC	CGCGGATCCGCGCCGCTTTGTCCTGGAC	[36]
BHRF1	GCAGGACATTGTGTTGTAACCAG	TAATGTAGACCAGCCGCCCT	[37]
BRLF1	GCTCAGGTCCATCTGTCCAC	GGGAGATGGCTGACACTGTT	[35]
BMRF1	GCGAGGAAAAGGACATCGT	CTTCACTTTCTTGGGGTGCT	[35]
BLLF1	CATCTACAGATTCCAGGCTTACTTG	AGCTTCCAATTAACGTCACCA	[35]
BZLF1	CCGGCTTGGTTAGTCTGTTG	AGCTTATGCAGCACCTCAGC	[35]
β-ACTIN	CAGAGCAAGAGAGGCATCCT	GGATAGCACAGCCTGGATAG	[31]
CD80	CCTCTCCATTGTGATCCTGG	GGCGTACACTTTCCCTTCTC	[38]
CD81	GTATTTTGGCAGGACCAGGA	GCCGCTTCTTCTTCTTCCAT	[38]
PD-L1	TTGGGAAATGGAGGATAAGA	GGATGTGCCAGAGGTAGTTCT	[39]
PD-L2	GTCTTGGGAGCCAGGGTGAC	TGAAAAGTGCAAATGGCAAGC	[40]
CEACAM1	TTCTGCATTTCGGGAAGACCGGCAG	AGCCCTGGAGATGCCTATTAG	[41]
Galectin-9	GGACGGACTTCAGATCACTGT	CCATCTTCAAACCGAGGGTTG	[42]
HLA-A	CGACGCCGCGAGCCAGA	GCGATGTAATCCTTGCCGTCGTAG	[43]
HLA-E	TGCGCGGCTACTACAATCAG	TGTCGCTCCACTCAGCCTTC	[44]
HLA-DR	GTTTACGACTGCAGGGTGGA	CCATCACCTCCATGTGCCT	[45]
Nectin-2	CGGAACTGTCACTGTCACCA	GACACTTCAGGAGGGTAGCG	[46]
PVR	CACTCAGGCATGTCCCGTAA	CATGCTCTGTACTCGAGGGA	[46]
HMGB1	ATATGGCAAAAGCGGACAAG	AGGCCAGGATGTT CTCCTTT	[47]

as follows: Scoring algorithm: Tanabe; Mode: Non-empty markers; Score filter: 60 %; Minimum markers: 8; and Maximum results: 200.

2.12. Statistical analysis

Statistical data was analyzed using the GraphPad Prism software. All data were presented as mean ± standard deviation. A *t*-test was used to compare the two groups of variables, with a difference considered statistically significant when $p < 0.05$.

3. Results

3.1. Usage of C666–1 and C17 cells in biomedical research

There has been a total of 1094 publications reporting results using the C666-1 cell line, emphasizing the significance and usefulness of this cell line for NPC research. Additionally, there have been 273 publications presenting findings using the C17 xenograft and the C17 cell line. These studies involving both cell lines contribute to a deeper understanding of NPC (Fig. S1).

3.2. STR similarity search

Initially, we conducted an STR profile analysis to verify the authenticity of the cell lines C17 and C666-1 used in our study. The results from the 16 STR marker CellCheck™ panel were then used to perform an STR similarity search with the CLASTR similarity search tool (Table S1). In both cases, the analyzed markers showed over an 80 % match to the previously reported STR profiles of these cells. It is important to note that for the cell line C666-1 three slightly different STR profiles were documented in the literature [50–52], all showing minor variations in some markers, suggesting a potentially highly unstable genome for this cell line. The STR profile of the C17 cell line had one variation at marker D8S1179. Although a previous report by Yip and colleagues [23] identified a tri-allelic pattern at that specific site (11, 14, and 15 repetitions), we only observed two (11 and 15 repetitions). However, our analysis confirmed that the STR profile we obtained for both cell lines had an 80 % match, indicating that both cell lines can be considered authentic.

3.3. Phenotypic appearance of C666–1 and C17 cells

Both NPC cell lines, exhibited a preference for growing in cell clusters (Fig. 1).

When grown at higher density, the cells produce cell clusters with distinct morphological characteristics, forming tightly packed, spherical aggregates. This is in contrast to the more flattened and spread-out morphology of the cells when grown at lower density.

Our observations have shown that the average doubling time for these cell lines varies, reflecting their unique growth dynamics. The C17 cell line has an average doubling time of approximately 6 days, indicating a relatively slower proliferation rate. On the other hand, the C666-1 cell line has a faster average doubling time of around 3.5 days, suggesting a more rapid growth rate (Fig. 2). These differences in doubling times are crucial for experimental planning and understanding the growth kinetics of each cell line. Overall, both the C666–1 and C17 cells grow as monolayers and spheroids, which is a common feature, but their growth rates differ *in vitro* [13,23].

3.4. Gene expression in NPC cells under basal culture conditions as determined by next generation mRNA sequencing

To analyze gene expression across the transcriptome, bulk mRNA sequencing (mRNA-Seq) was conducted on both cell lines using next-generation sequencing (NGS). Total RNA was extracted from cells grown in basal medium. In the C17 cell line, 39,342 distinct transcript species were identified, while the C666-1 cell line had 28,350 different transcript species. Notably, both cell lines shared 27,374 identical transcripts (Table S2).

Based on previous studies [53–57], we have selected 49 genes of interest whose expression may play a role in NPC tumorigenesis. These genes include for example epithelial cell adhesion molecule (*EpCAM*), *ERBB2* (also known as *HER2*), epidermal growth factor receptor (*EGFR*), and *B7H3/CD276*, also known as CD276. Most of these genes were expressed in both NPC cell lines (C666–1 and C17). However, fibroblast growth factor receptor 1 (*FGFR1*), Glutathione S-transferase A3 (*GSTA3*), receptor tyrosine kinase RET (*RET*), and ubiquitin carboxy-terminal hydrolase L1 (*UCHL1*) were exclusively found in the C17 cell line, with no expression observed in the C666-1 cell line (Table 2).

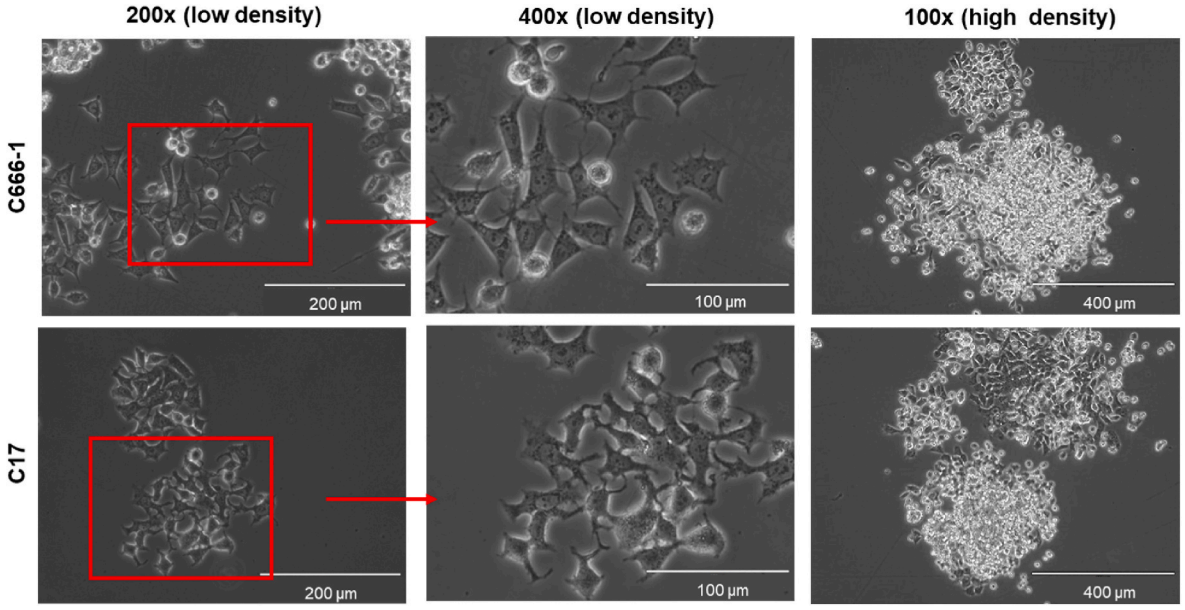

Fig. 1. Light microscopic appearance of C17 and C666-1 cells. The cells were seeded in cell culture dishes and representative images were captured. Original magnifications are depicted.

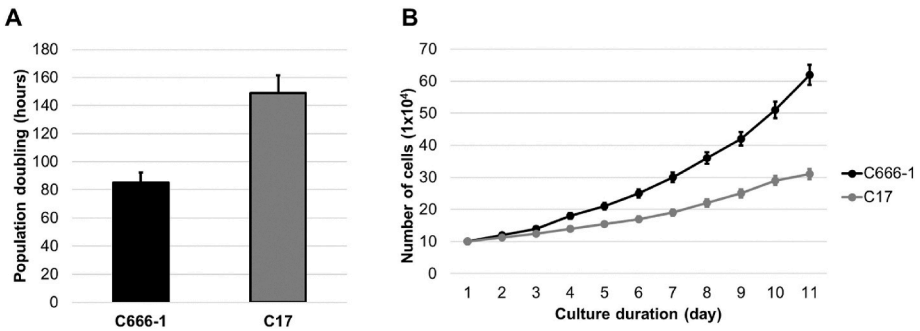

Fig. 2. Cell growth and population doubling time of C666–1 and C17 cells. (**A**) Population doubling time and (**B**) cell proliferation rate of both NPC cell lines in complete cell growth media are presented. The data is from three independent experiments and is presented as mean ± SD.

Table 2
Genes with potential roles in NPC tumorigenesis found in C17 and C666-1 cell lines through RNA-Seq analysis.

Gene_ID	Gene_Name	C17[a]	C666-1[a]	References
ENSG00000097007.20	*ABL1*	483.02	859.73	[57]
ENSG00000142208.18	*AKT1*	695.08	1183.45	[57]
ENSG00000105221.18	*AKT2*	918.92	683.40	[54]
ENSG00000117713.21	*ARID1A*	948.91	1099.23	[54]
ENSG00000163930.10	*BAP1*	630.82	579.88	[54]
ENSG00000157764.14	*BRAF*	1194.17	967.64	[54]
ENSG00000103855.18	*CD276*	1087.07	707.09	[54]
ENSG00000135446.17	*CDK4*	891.07	1535.24	[57]
ENSG00000147889.18	*CDKN2A*	208,85	36,85	[54]
ENSG00000117322.19	*CR2*	7.50	24.56	[54]
ENSG00000163734.4	*CXCL3*	52.48	472.85	[54]
ENSG00000119772.19	*DNMT3A*	763.62	941.32	[54]
ENSG00000088305.19	*DNMT3B*	36.41	30.70	[54]
ENSG00000146648.21	*EGFR*	3518.24	900.09	[57]
ENSG00000128886.12	*ELL3*	94.25	64.04	[54]
ENSG00000119888.11	*EpCAM*	2666.79	2871.34	[54]
ENSG00000141736.14	*ERBB2*	664.02	1210.65	[57]
ENSG00000106462.12	*EZH2*	355.57	219.32	[54]
ENSG00000077782.23	*FGFR1*	188.50	0.00	[57]
ENSG00000068078.20	*FGFR3*	167.08	62.29	[57]
ENSG00000122025.15	*FLT3*	4.28	24.56	[57]
ENSG00000075420.13	*FNDC3B*	2643.23	1962.48	[54]
ENSG00000141448.11	*GATA6*	65.33	172.82	[54]
ENSG00000174156.15	*GSTA3*	13.92	0.00	[54]
ENSG00000068024.18	*HDAC4*	451.96	176.33	[54]
ENSG00000174775.18	*HRAS*	183.14	206.16	[57]
ENSG00000090339.9	*ICAM1*	5925,85	4727,66	[54]
ENSG00000096968.14	*JAK2*	964.97	447.41	[57]
ENSG00000173801.17	*JUP*	4020.54	1762.46	[54]
ENSG00000157404.17	*KIT*	237.76	1.75	[57]
ENSG00000272333.8	*KMT2B*	399.48	449.17	[54]
ENSG00000055609.21	*KMT2C*	3588.93	3782.83	[54]
ENSG00000167548.18	*KMT2D*	1592.58	1368.56	[54]
ENSG00000133703.14	*KRAS*	985.32	880.79	[57]
ENSG00000086730.17	*LAT2*	43.91	36.85	[54]
ENSG00000106689.11	*LHX2*	82.47	41.23	[54]
ENSG00000105976.16	*MET*	1041.01	408.81	[57]
ENSG00000181143.16	*MUC16*	273.11	1815.09	[54]
ENSG00000213281.5	*NRAS*	864.30	3710.90	[57]
ENSG00000157212.20	*PAXIP1*	311.66	455.31	[54]
ENSG00000134853.12	*PDGFRA*	312.73	107.03	[54]
ENSG00000121879.6	*PIK3CA*	934.98	439.52	[54]
ENSG00000198901.14	*PRC1*	687.58	590.41	[54]
ENSG00000165731.21	*RET*	18.21	0.00	[57]
ENSG00000019549.13	*SNAI2*	181.00	14.91	[54]
ENSG00000124766.7	*SOX4*	1761.80	1884.40	[54]
ENSG00000178691.11	*SUZ12*	2685.00	2059.85	[54]
ENSG00000121297.8	*TSHZ3*	100.67	33.34	[54]
ENSG00000154277.13	*UCHL1*	41.77	0.00	[54]

[a] Read counts for each gene in the sample utilized for RNA-Seq analysis.

The genes listed in Table 2 are also displayed in a heatmap (Fig. 3) for easy visual comparison of expression levels between C17 and C666-1 cells. This color-coded display effectively highlights significant differences, making it easier to identify upregulated or downregulated genes in each cell line. Additionally, it visually represents the expression levels of these genes, with highly expressed genes marked in red, moderately expressed genes in yellow, and genes with low expression in blue.

Since the RNA-Seq data was collected from only one experiment, we were unable to conduct statistical analysis based on our initial findings. To validate the data, we subsequently selected a few genes and confirmed the RNA-Seq results using either FACS analysis or RT-qPCR. For FACS analysis, we focused on the following genes: *EpCAM, ERBB2, EGFR, ICAM1* and *B7H3/CD276*. Both cell lines demonstrated significant surface expression of *EpCAM, ERBB2, EGFR, ICAM1* and *B7H3/CD276*. This finding, combined with the RNA-Seq data and short tandem repeat profiling, confirms that the C666–1 and C17 cell lines belong to the carcinoma cell line family. Additionally, the similarity of the results between the EBV-negative NPC cell line HK1 and both EBV-positive NPC cell lines C17 and C666-1 eliminates any suggestion that the observed outcome is a result of EBV infection (Fig. 4).

In our efforts to confirm the unique characteristics of each cell line, we analyzed RNA-Seq data to identify genes specific to each line (Table S3). Through this analysis, we discovered 11,968 transcripts unique to C17 and 976 transcripts unique to C666-1. This indicates that C17 had approximately 25 % more transcripts than C666-1 (Fig. 5).

As mentioned earlier, specific genes such as *FGFR1, GSTA3, RET*, and *UCHL1* were exclusively expressed in the C17 cell line, with no expression in the C666-1 cell line. These differential gene expressions highlight the unique molecular profiles of the two cell lines. These findings were confirmed using RT-qPCR (Table 3, Fig. 6). The mean relative mRNA values for *FGFR1* and *RET* in cell line C17 were 22.94 ± 3.69 and 121.33 ± 26.30, respectively, indicating moderate gene expression compared to *GSTA3* (3198.27 ± 147.00) and *UCHL1* (1628.20 ± 294.14), which showed strong expression. The mean relative mRNA values for all genes in C666-1 were around 1.00, indicating no gene expression in this cell line.Table. 4

To assess the similarity between the C666–1 and C17 cell lines and NPC (NPC tissue from 10 patients), we compared their gene expression profiles. However, it is worth to note that our cell line samples were analyzed using bulk total RNA-seq, while the dataset from GSE61218 [58] was profiled using a microarray platform. Therefore, a direct comparison of absolute expression levels is challenging. Nevertheless, to address this, we ranked the genes from Fig. 3 in both datasets based on their expression levels. Within each sample, the gene with the highest expression was assigned a rank of 1.0, facilitating a relative comparison across datasets. This analysis demonstrated that out of 41 analyzed genes, only *FGFR3*, *CDKN2A*, *LAT2*, and *SNAI2* showed significant differences between both cell lines and NPC tissue (Fig. 7). This indicates that C666–1 and C17 cells have strong similarities with NPC tissue. These findings suggest that the genetic profiles of C666–1 and C17 cells

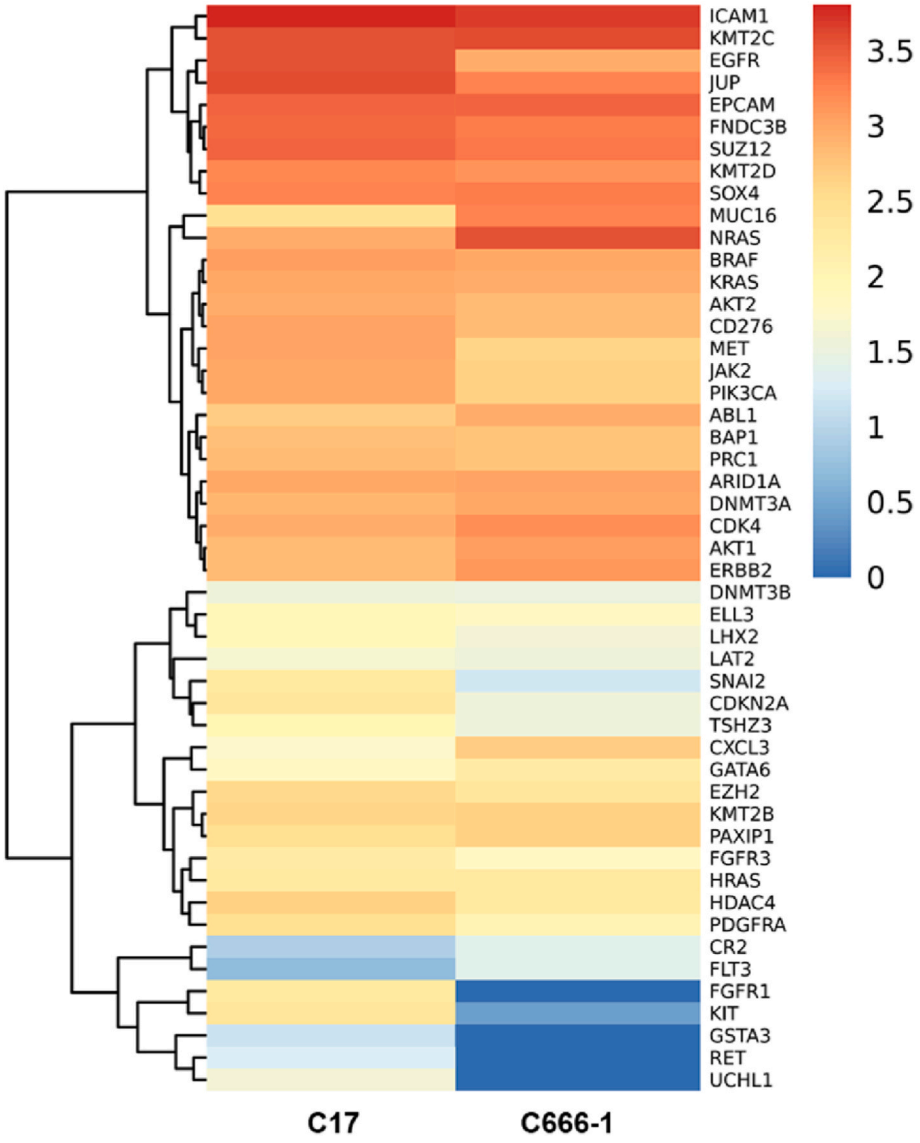

Fig. 3. Heatmap of genes, potentially involved in NPC tumorigenesis, identified in C17 and C666-1 cell lines through RNA-Seq analysis (see also Table 2). The columns represent samples, while the rows represent genes. Clustering of samples and genes is depicted by dendrogram trees. Samples or genes that are grouped closer together are illustrated with fewer branch points in the dendrogram. The color scheme indicates gene expression levels in either C17 or C666-1 cells, with blue indicating low expression, yellow indicating moderate expression, and red indicating high expression. (For interpretation of the references to color in this figure legend, the reader is referred to the Web version of this article.)

closely resemble those of NPC tissue, making them valuable models for studying the molecular mechanisms underlying NPC.

3.5. EBV status and EBV gene expression in NPC cells under basal culture conditions as determined by next generation mRNA sequencing

We have previously demonstrated that the culture supernatants of C666–1 and C17 contain a significant amount of EBV-DNA [24]. Despite these findings, we were unable to detect the production of viral particles within the cells. To further investigate this, we used electron microscopy (Fig. 8). The electron microscopy analysis was performed to generate high-resolution images of the cellular structures, with the goal of identifying any viral particles that may be present. However, even with this advanced imaging technique, no viral particles were observed within the cells. This suggests that, under the conditions tested, the cells did not produce detectable levels of viral particles, indicating a potential block in the viral replication cycle or an absence of active viral infection in these cell lines.

Through a detailed RNA-Seq analysis, we aimed to explore the specific EBV gene profiles of the C666–1 and C17 cell lines. We identified the expression of 65 EBV genes in total, with 58 genes expressed in the C666-1 cell line and 53 in the C17 cell line (Fig. 9).

In both cell lines, these transcripts included 11 latency genes and 54 lytic genes (Table 5).

The genes listed in Table 5 are further illustrated in a visual representation using a heatmap (Fig. 10), facilitating a side-by-side comparison of gene expression levels between C19 and C666-1 cells.

In NPC, EBV infection typically presents with a type II latency pattern, which includes the expression of Epstein-Barr nuclear antigen 1 *(EBNA1)*, latent membrane proteins *(LMP)* 1 and 2, and non-coding RNAs [13,23]. Our initial focus was to identify the most distinctive EBV genes associated with latent infection in NPC. In our experiments, both cell lines showed expression of the latency-associated genes *EBNA1* and *LMP2*. Additionally, the C17 cell line uniquely expressed *LMP1*, an oncogenic and immune evasion gene, and *EBNA2*, which plays a role in B cell transformation and works with *LMP1* to immortalize infected

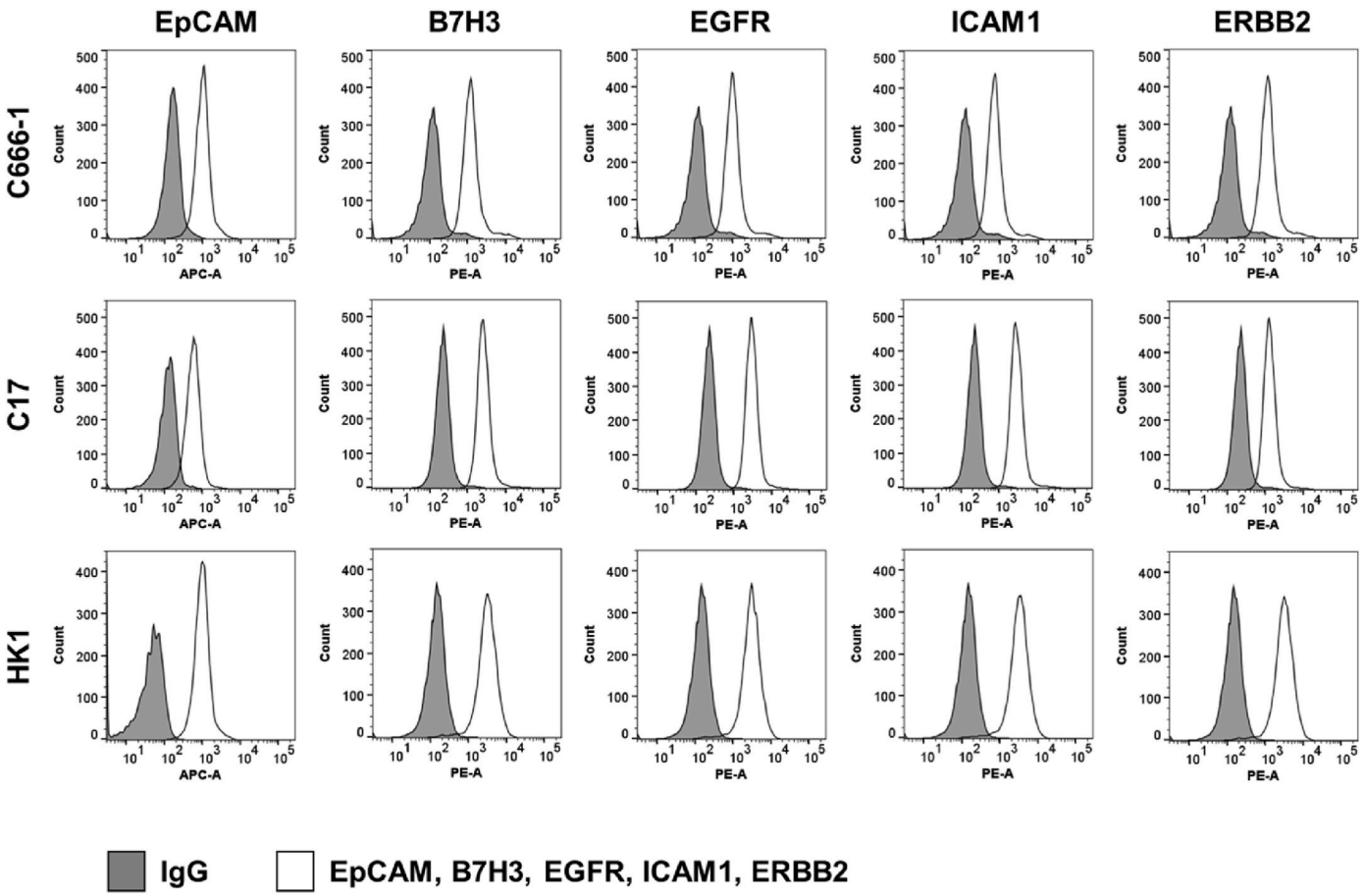

Fig. 4. Surface expression of EpCAM, B7H3/CD276, EGFR, ICAM1, and ERBB2 on cell lines C666–1, C17 and HK1. Each cell line was stained with antibodies for EpCAM, B7H3/CD276, EGFR, ICAM1, and ERBB2, as well as their corresponding IgGs. Pro sample IgGs were prepared only once and used as controls for other stainings with the same fluorochrome. The expression of each protein was assessed using flow cytometry following the manufacturer's protocol.

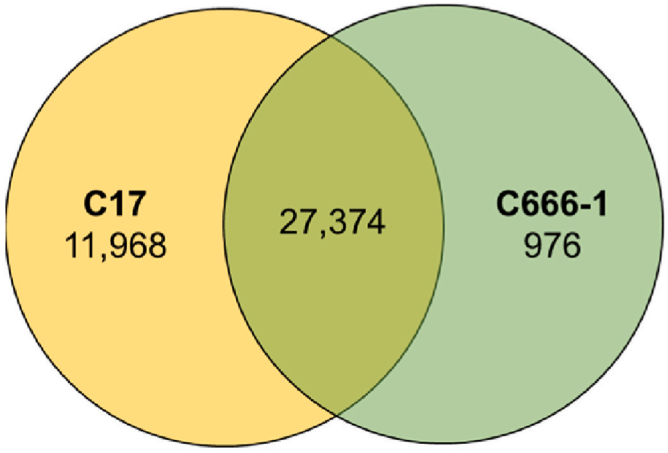

Fig. 5. Venn diagram illustrating the differentially expressed genes (DEGs) in NPC cell lines, highlighting both unique and overlapping DEGs. The C17 cell line had 39,342 transcript species, while the C666-1 cell line had 28,350 transcript species. Both cell lines shared 27,374 identical transcripts, with 11,968 unique to C17 and 976 unique to C666-1.

cells. Both cell lines demonstrated the expression of type III latent genes: *EBNA3A, EBNA3B*, and *EBNA3C*. The expression of *EBNA3A* is slightly higher in the C666-1 cell line than in the C17 cell line.

Furthermore, both cell lines expressed the BART genes *RPMS1* and *A73*, as well as the regulatory and oncogenic gene *BARF0*. Next, we

Table 3
Differences between two cell lines based on example genes as determined by RNA-Seq.

Gene_ID	Gene_Name	C17[a]	C666-1
ENSG00000077782.23	*FGFR1*	188.50	0
ENSG00000174156.15	*GSTA3*	13.92	0
ENSG00000165731.21	*RET*	18.21	0
ENSG00000154277.13	*UCHL1*	41.77	0

[a] Read counts for each gene in the sample utilized for RNA-Seq analysis.

examined the expression of EBV lytic genes in both cell lines. Forty-nine lytic genes were expressed in the C666-1 cell line, and forty-two lytic genes were found in the C17 cell line. The gene kinetics demonstrated that in C666-1 cell line, two lytic genes belong to immediate early genes (*BRLF1* and *BZLF2*), twenty-three are early genes, and twenty-four are late genes. In C17, there is only one immediate early gene (*BRLF1*), twenty early genes, and twenty-one late genes. In the context of the known EBV lytic genes found in NPC tissue [13,23], we observed that late genes such as *BHRF1* and *BZLF2* were found in both cell lines. The expression of *BHRF1* was higher in C666-1 than in C17, compared to *BZLF2*, where the gene expression was higher in C17. Two early genes, *BMRF1* and *BLLF1*, were expressed in both cell lines, but their expression was lower in C17 cells compared to C666-1. Additionally, we noted that the lytic cycle gene *BZLF1* was present in the C666-1 cell line, while *BZLF2* was found in both cell lines.

Quantitative RT-PCR analysis of the EBV gene expression profile indicated high levels of gene expression for latent EBV genes, including

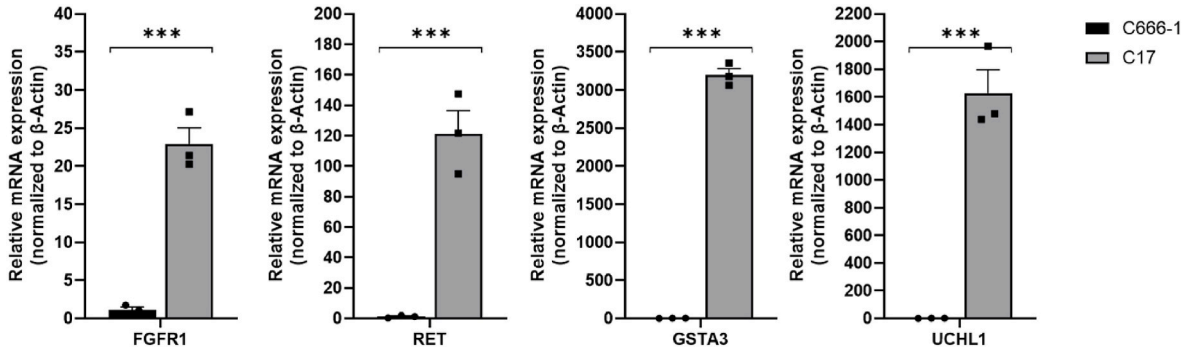

Fig. 6. Gene expression analysis in C666–1 and C17 cells. RT-qPCR analysis was conducted on genes associated with the unique characteristics of these cell lines. The expression of the genes analyzed was normalized to β-actin expression. The data are presented as mean ± SD (n = 3 independent assays). Asterisks denote statistically significant differences between the two cell lines (**$p < 0.01$; ***$p < 0.001$).

Table 4
Rank of genes with potential roles in NPC tumorigenesis identified in C17 and C666-1 cell lines in comparison to NPC tissue.

Gene_ID	Gene_Name	C17[a]	C666-1[a]	NPC Tissue[a]									
				T2-1	T2-2	T2-3	T3-1	T3-2	T3-3	T3-4	T3-5	T4-1	T4-2
ENSG00000097007.20	*ABL1*	0.71	0.80	0.65	0.72	0.75	0.72	0.57	0.66	0.44	0.56	0.66	0.64
ENSG00000142208.18	*AKT1*	0.79	0.86	1.00	1.00	1.00	1.00	1.00	1.00	1.00	1.00	1.00	1.00
ENSG00000105221.18	*AKT2*	0.84	0.75	0.67	0.64	0.66	0.66	0.61	0.57	0.64	0.63	0.62	0.65
ENSG00000117713.21	*ARID1A*	0.84	0.85	0.90	0.87	0.91	0.85	0.86	0.71	0.84	0.83	0.89	0.89
ENSG00000163930.10	*BAP1*	0.77	0.71	0.66	0.68	0.68	0.72	0.78	0.65	0.67	0.82	0.76	0.82
ENSG00000157764.14	*BRAF*	0.88	0.82	0.91	0.92	0.90	0.91	0.92	0.93	0.92	0.94	0.91	0.90
ENSG00000103855.18	*CD276*	0.87	0.76	0.66	0.66	0.73	0.78	0.74	0.77	0.68	0.65	0.70	0.60
ENSG00000135446.17	*CDK4*	0.83	0.90	0.93	0.95	0.97	0.94	0.96	0.97	0.95	0.96	0.95	0.95
ENSG00000147889.18	*CDKN2A*	0.52	0.28	0.93	0.97	0.93	0.95	0.93	0.97	0.95	0.94	0.96	0.95
ENSG00000117322.19	*CR2*	0.09	0.25	0.43	0.15	0.06	0.08	0.19	0.09	0.08	0.26	0.14	0.53
ENSG00000163734.4	*CXCL3*	0.31	0.66	0.19	0.48	0.45	0.81	0.62	0.64	0.18	0.68	0.17	0.11
ENSG00000119772.19	*DNMT3A*	0.80	0.82	0.69	0.78	0.66	0.65	0.66	0.70	0.66	0.75	0.63	0.66
ENSG00000088305.19	*DNMT3B*	0.27	0.27	0.03	0.07	0.06	0.04	0.07	0.08	0.04	0.06	0.05	0.06
ENSG00000146648.21	*EGFR*	0.97	0.81	0.52	0.42	0.62	0.37	0.42	0.50	0.51	0.62	0.28	0.46
ENSG00000128886.12	*ELL3*	0.38	0.33	0.38	0.17	0.14	0.13	0.17	0.21	0.35	0.41	0.22	0.46
ENSG00000119888.11	*EpCAM*	0.96	0.96	0.78	0.91	0.94	0.81	0.93	0.92	0.92	0.83	0.95	0.72
ENSG00000141736.14	*ERBB2*	0.78	0.86	0.66	0.68	0.63	0.67	0.70	0.74	0.71	0.76	0.63	0.69
ENSG00000106462.12	*EZH2*	0.64	0.49	0.12	0.19	0.19	0.17	0.15	0.12	0.19	0.07	0.14	0.13
ENSG00000077782.23	*FGFR1*	0.73	0.67	0.50	0.47	0.44	0.45	0.51	0.51	0.46	0.49	0.43	0.51
ENSG00000068078.20	*FGFR3*	0.48	0.32	0.59	0.78	0.95	0.53	0.85	0.65	0.81	0.70	0.51	0.73
ENSG00000122025.15	*FLT3*	0.05	0.25	0.24	0.08	0.09	0.11	0.07	0.09	0.07	0.02	0.08	0.14
ENSG00000075420.13	*FNDC3B*	0.96	0.93	0.88	0.80	0.87	0.92	0.87	0.85	0.85	0.80	0.87	0.85
ENSG00000141448.11	*GATA6*	0.34	0.45	0.09	0.10	0.10	0.04	0.10	0.12	0.11	0.16	0.07	0.06
ENSG00000068024.18	*HDAC4*	0.69	0.45	0.43	0.48	0.42	0.48	0.40	0.39	0.41	0.45	0.45	0.35
ENSG00000174775.18	*HRAS*	0.50	0.48	0.42	0.47	0.61	0.64	0.60	0.63	0.61	0.64	0.47	0.51
ENSG00000090339.9	*ICAM1*	0.99	0.98	0.97	0.97	0.98	0.97	0.90	0.95	0.93	0.97	0.88	0.94
ENSG00000096968.14	*JAK2*	0.85	0.65	0.72	0.83	0.68	0.63	0.55	0.87	0.64	0.87	0.56	0.80
ENSG00000173801.17	*JUP*	0.98	0.92	0.89	0.89	0.97	0.93	0.93	0.92	0.91	0.96	0.92	0.94
ENSG00000157404.17	*KIT*	0.55	0.07	0.71	0.98	0.36	0.45	0.78	0.34	0.44	0.55	0.71	0.58
ENSG00000133703.14	*KRAS*	0.85	0.80	0.44	0.43	0.43	0.51	0.49	0.44	0.39	0.49	0.54	0.45
ENSG00000086730.17	*LAT2*	0.29	0.28	0.85	0.80	0.74	0.80	0.80	0.77	0.76	0.83	0.73	0.86
ENSG00000106689.11	*LHX2*	0.36	0.29	0.27	0.44	0.89	0.77	0.51	0.81	0.53	0.60	0.40	0.53
ENSG00000105976.16	*MET*	0.86	0.63	0.25	0.23	0.56	0.48	0.41	0.11	0.12	0.24	0.44	0.22
ENSG00000181143.16	*MUC16*	0.58	0.92	0.77	0.70	0.65	0.48	0.57	0.55	0.50	0.63	0.72	0.61
ENSG00000213281.5	*NRAS*	0.83	0.97	0.90	0.92	0.92	0.88	0.90	0.89	0.92	0.83	0.83	0.89
ENSG00000157212.20	*PAXIP1*	0.60	0.65	0.72	0.71	0.76	0.80	0.71	0.66	0.70	0.56	0.78	0.65
ENSG00000134853.12	*PDGFRA*	0.61	0.38	0.57	0.50	0.74	0.52	0.57	0.51	0.35	0.26	0.38	0.35
ENSG00000121879.6	*PIK3CA*	0.84	0.65	0.61	0.49	0.65	0.55	0.58	0.55	0.57	0.56	0.62	0.59
ENSG00000198901.14	*PRC1*	0.60	0.84	0.66	0.73	0.78	0.66	0.70	0.72	0.71	0.67	0.66	0.74
ENSG00000019549.13	*SNAI2*	0.49	0.22	0.79	0.82	0.86	0.87	0.84	0.83	0.85	0.84	0.85	0.76
ENSG00000124766.7	*SOX4*	0.92	0.92	0.59	0.89	0.89	0.75	0.82	0.75	0.65	0.72	0.73	0.67
ENSG00000178691.11	*SUZ12*	0.96	0.93	0.58	0.64	0.77	0.68	0.56	0.66	0.69	0.55	0.67	0.53
ENSG00000121297.8	*TSHZ3*	0.39	0.27	0.16	0.11	0.15	0.36	0.21	0.16	0.10	0.06	0.20	0.10

[a] Depicted is the rank for each gene in the sample.

EBNA1, EBER1/2, LMP1, LMP2, BRLF1, BMRF1, BLLF1, and *BZLF1* in both cell lines. However, these genes were expressed at lower levels in the C666-1 cell line compared to the C17 cells (Fig. 11). This discrepancy in gene expression levels between the two cell lines suggests potential variations in the biological behavior or cellular environment of both cell lines, which could influence the overall viral persistence within these cells.

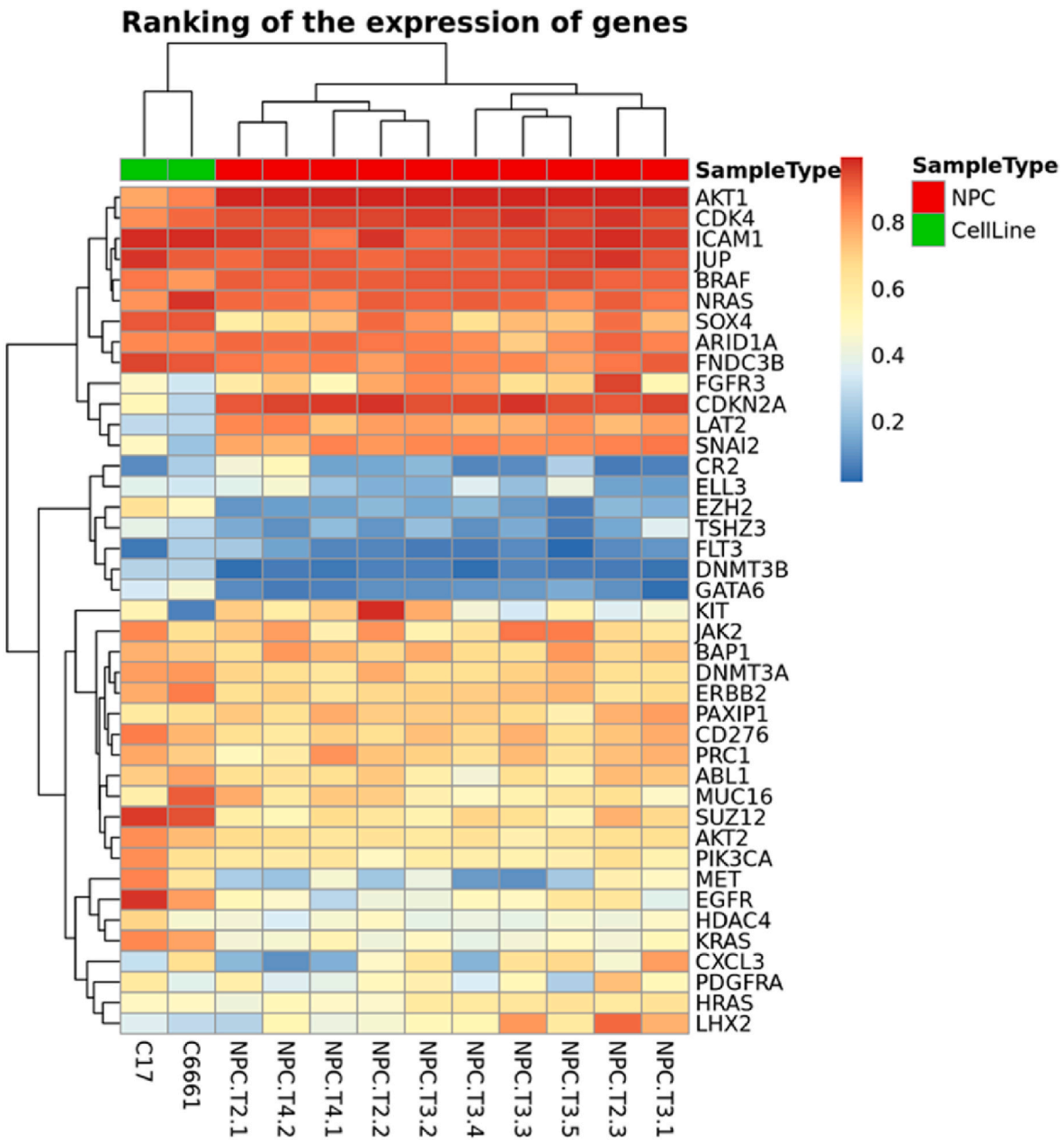

Fig. 7. Heatmap of genes, potentially involved in NPC tumorigenesis, identified in the C666–1 and C17 cell lines, as well as nasopharyngeal carcinoma (NPC tissue from 10 patients) (see also Table 4). This comparison was performed using R 4.3. leveraging, the GEOquery package for data retrieval, and pheatmap for visualization. The columns represent samples, while the rows represent genes. Clustering of samples and genes is depicted by dendrogram trees. Samples or genes that are grouped closer together are illustrated with fewer branch points in the dendrogram. The color scheme indicates gene expression levels in either C17 or C666-1 cells, with blue indicating low expression, yellow indicating moderate expression, and red indicating high expression.

3.6. Expression of genes related to escape from immune surveillance in NPC cells under basal culture conditions as determined by next-generation mRNA sequencing

NPC is a highly immune-inflamed cancer, primarily due to chronic EBV infection [1]. In this study, we present the results of an investigation into the expression of genes related to immune escape mechanisms in two NPC cell lines: C666–1 and C17. The expression levels were assessed using RNA sequencing (RNA-Seq) (Table 6), PCR (Fig. 12), and flow cytometry (Fig. S2). RNA-Seq analysis identified 24 genes of interest, including many checkpoint genes and various *HLA* genes. The expression levels of these genes in the two cell lines are summarized below. *PD-L1* (CD274), *CD80*, *CD86*, *CEACAM1*, *NECTIN2* (PVRL2), and *PVR* were expressed at higher levels in C666-1 compared to C17. Interestingly *PD-L2* (PDCD1LG2) was expressed only in the C17 cell line. On the other hand, *Galectin-9* (LGALS9) and *HLA-G* showed higher expression in C17 compared to C666-1. Other genes such as *HMGB1* and the rest of the *HLA* genes demonstrated very high expression in both cell lines. Quantitative PCR (qPCR) was performed to validate the RNA-Seq results. The qPCR data confirmed the RNA-Seq findings, with consistent expression trends observed for the key genes.

The results from RNA-Seq, PCR, and flow cytometry collectively indicate that C666–1 may employ multiple mechanisms to evade immune detection, including the upregulation of *PD-L1*, *CD80*, *CD86*, and certain *HLA* molecules. In contrast, C17 appears to enhance immune activation through the expression of *PD-L2*, *Galectin-9*, and other *HLA* genes. These findings provide valuable insights into the immune escape strategies of different cell lines and may inform therapeutic approaches

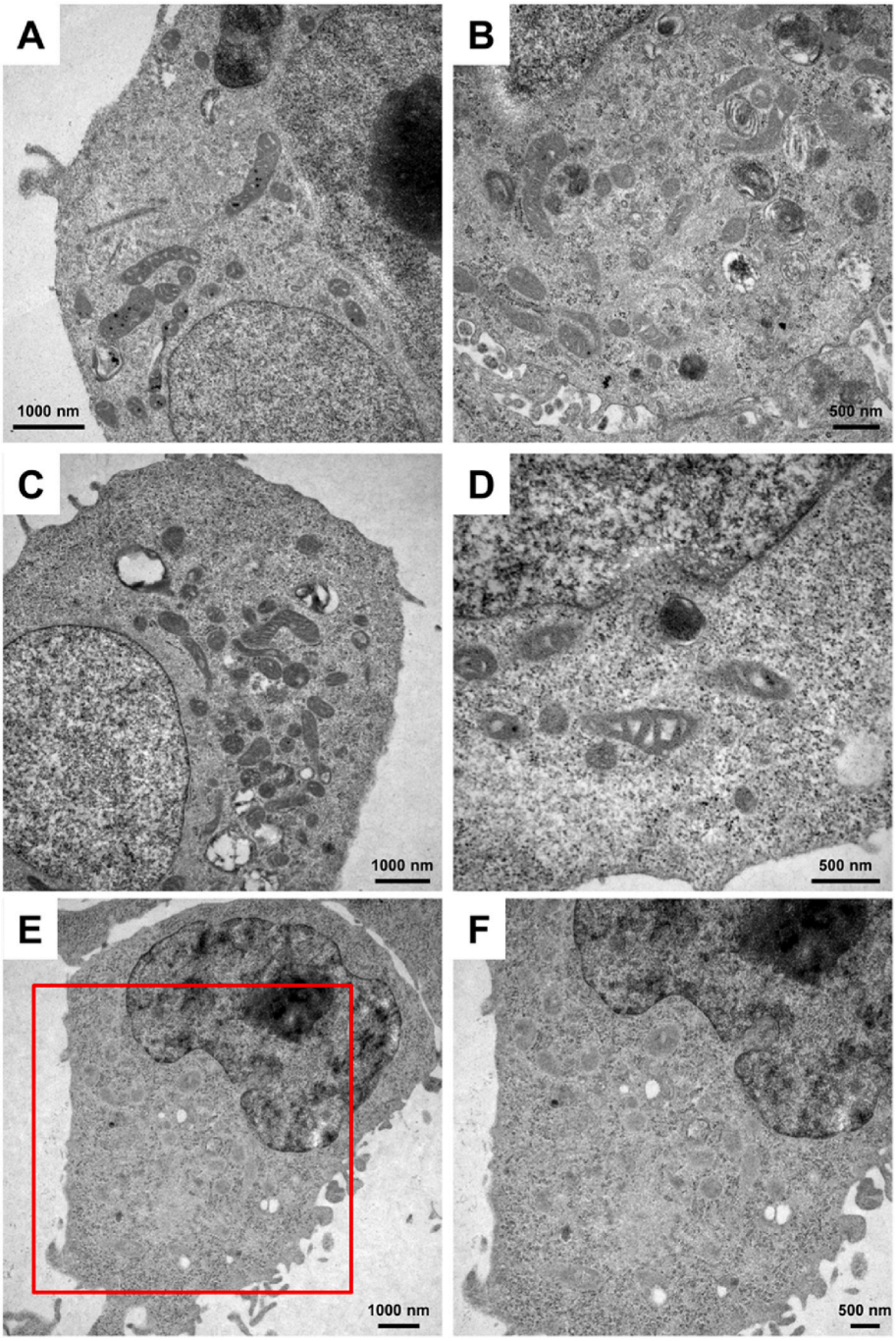

Fig. 8. Transmission electron microscopy. Photomicrographs show normal nuclear and intracellular morphologies in C17 (**A, B**), C666-1 (**C, D**) and HK1 (**E, F**) cell lines. No viral particles were observed in both NPC cell lines. Please note that panel (**F**) is a magnification of panel (**E**).

targeting these pathways. This study highlights the importance of integrating multiple techniques to comprehensively analyze gene and protein expression related to immune escape mechanisms. The differential expression patterns observed in the two cell lines underscore the complexity of immune evasion and the potential for targeted therapies to overcome these challenges.

Next, we examined the similarity of genes related to immune escape mechanisms between the C666–1 and C17 cell lines and nasopharyngeal carcinoma (NPC) patient tissues. The genetic characteristics identified in our cell lines were validated using transcriptomic datasets: GSE68799, GSE102349, and GSE118719 (Fig. 13, Fig. S3, Table S4) [60,61]. Each dataset was compared with our cell lines individually. This analysis showed that both C666–1 and C17 displayed a strong similarity to NPC tissue. Validating these genetic features through transcriptomic datasets strengthens the reliability of our findings.

4. Discussion

In this study, we compare the C666–1 and C17 cell lines using bulk RNA-Seq. This method reveals genetic and epigenetic changes. Furthermore, we identify EBV gene transcripts in both cell lines, which can help in understanding NPC pathogenesis.

The expression of EBV genes in NPC and other EBV-associated carcinomas varies depending on the type of carcinoma and the latency program of the virus [62,63]. In the context of NPC, the expression pattern of EBV genes is characterized by Latency Type II, which involves

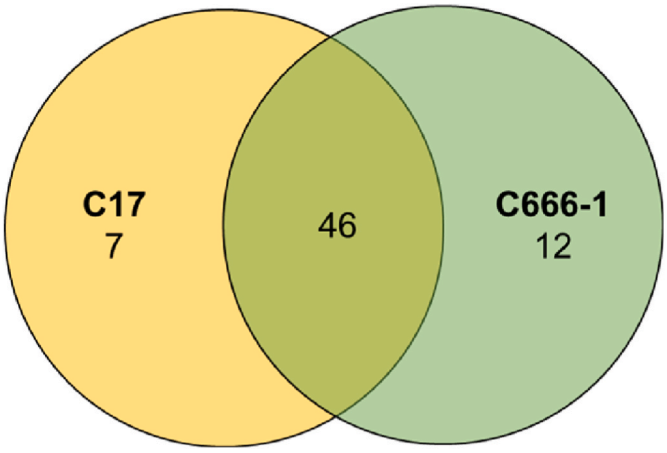

Fig. 9. Venn diagram illustrating the differentially expressed EBV genes (DEGs) in NPC cell lines, highlighting both unique and overlapping DEGs. The C17 cell line had 53 transcript species, while the C666-1 cell line had 58 transcript species. Both cell lines shared 46 identical transcripts, with 7 unique to C17 and 12 unique to C666-1.

the expression of *EBNA1, LMP1, LMP2A/B,* and *EBERs* (EBV-encoded small RNAs) [64]. These genes are essential for maintaining the viral genome and promoting the survival and proliferation of infected cells [14,20,63]. This limited gene expression profile contrasts with latency type III, which encompasses a broader range of EBV genes, including EBNA3s and a substantial number of lytic genes such as *BZLF1*, *BRLF1*, and *BMRF1* [65]. In our experiments, we were able to confirm the expression of Latency Type II and III EBV genes in both cell lines. In comparison, other EBV-associated carcinomas, such as gastric carcinoma (Latency type I or II) and Hodgkin lymphoma, typically exhibit a Latency Type II with *EBNA1*, *LMP1*, *LMP2A/B*, and *EBERs* commonly expressed [64–66]. However, Hodgkin lymphoma generally shows the expression of *EBNA1*, *LMP1*, and *LMP2A* [66]. Burkitt lymphoma is primarily associated with Latency Type I. In this latency type, the viral genes EBNA1 and the EBERs are expressed, while the latent membrane proteins LMP1 and LMP2 are not expressed [65].

As mentioned before, although NPC is typically characterized by latency type II, our experiments detected type III latency genes in both cell lines: C666–1 and C17. Hu et al. demonstrated in their study that the detection of type III latency genes in C666-1 is not an isolated event. In their research, four out of twelve NPC tissue samples expressed type III latency genes. The same authors showed the presence of *EBNA2* transcripts in C666-1 but were unable to detect any protein expression. In our experiments, we couldn't detect *EBNA2* and *LMP2* transcripts in the C666-1 cell line. However, *EBNA3C* was expressed in both cell lines. Recent studies have revealed that EBNA3C significantly contributes to oncogenesis by impairing DNA damage signaling and facilitating the transformation of cells by EBV. Consequently, the expression of latency genes in NPC is not strictly limited to the type II latency pattern [66].

In our experiment, we demonstrated that both cell lines expressed a significant number of EBV lytic genes. The transition from latent to lytic EBV infection results in viral replication, production of new viral particles, and ultimately, lysis of infected cells. The lytic cycle is divided into three stages: immediate early, early, and late [67]. In the C17 cell line, we identified only one immediate early gene, *BRLF1*, whereas in the C666-1 cell line, we found two immediate early genes, *BRLF1* and *BZLF1*. Both genes function as immediate early transcription factors that activate EBV lytic gene expression. Early genes primarily facilitate viral DNA replication, while late genes are involved in viral particle assembly. *BZLF1* and *BRLF1* enhance the expression of early lytic genes, including those encoding components of the core replication machinery, such as *BALF5* (DNA polymerase), *BALF2* (single-stranded DNA-binding protein), *BMRF1* (DNA polymerase processivity factor), *BSLF1* (primase),

Table 5
EBV gene expression in C666–1 and C17 cells.

Latent Genes				
Gene ID	Gene symbol	C666-1[a]	C17[a]	Type [59]
gene135	*A73*	706.734922	27.429110	I, II, III
Q8AZJ4	*BARF0*	681.237496	19.010145	II
gene126	*RPMS1*	398.657439	12.555517	III
gene0	*LMP2*	46.901294	1.628548	II, III
P03179	*BNRF1 (LMP2)*	11.629434	2.886761	II, III
P03211	*BKRF1 (EBNA1)*	4.074709	7.406157	I, II, III
gene152	*EBNA3A*	2.397444	1.226745	III
gene64	*EBNA3B*	1.206801	1.234997	III
gene66	*EBNA3C*	1.137785	1.164494	III
P03230	*LMP1*	0	2.160344	II, III
P12978	*BYRF1 (EBNA2)*	0	1.665483	III
Lytic Genes				
Gene ID	**Gene symbol**	**C666–1[a]**	**C17[a]**	**Type [59]**
gene71	*BZLF1*	29.934019	0	Immediate Early
gene70	*BRLF1*	9.157907	1.313864	Immediate Early
Q04360	*SM%2C spliced BSLF2+BMLF1*	115.223025	0.936855	Early
P03191	*BMRF1*	100.276024	2.051699	Early
P03227	*BALF2*	47.402169	2.375601	Early
Q777A5	*BARF1*	41.822077	0.000000	Early
P03190	*BORF2*	34.511968	2.353913	Early
P0C739	*BNLF2a*	29.951331	0	Early
Q777D9	*BKRF3*	23.310562	7.029893	Early
Q69117	*BFRF1A*	21.499654	4.110874	Early
P03217	*BGLF5*	17.810881	0.000000	Early
P03177	*BXLF1*	14.888411	7.200489	Early
Q777G2	*BORF1*	13.589155	2.309839	Early
P03207	*BRRF1*	13.306580	2.782447	Early
Q777C8	*BGLF2*	12.113771	3.799378	Early
P0C725	*LF2*	10.567697	0	Early
Q777C7	*BGLF1*	9.357642	0.796608	Early
P03195	*BLLF3*	9.326002	1.583182	Early
Q777B2	*BILF1*	8.126722	0.000000	Early
P13288	*BGLF4*	7.749645	0.958874	Early
Q777F5	*BSLF1*	7.151539	0.443488	Early
Q8AZJ7	*BBLF2-BBLF3*	5.568699	2.169667	Early
Q777G8	*BFLF1*	5.065141	2.300003	Early
Q777D7	*BBLF4*	3.175443	0.962546	Early
P03219	*BGRF1-BDRF1*	2.091013	1.710644	Early
Q777C3	*BDLF1*	0	4.321022	Early
Q777C4	*BDLF2*	0	4.321022	Early
P03182	*BHRF1*	39.319364	5.067216	Late
P30117	*BKRF4*	38.053012	8.592813	Late
P0CAP6	*BaRF1*	21.115437	2.869425	Late
Q777G5	*BFRF3*	18.819026	0.000000	Late
P03231	*BXLF2*	15.505413	3.894728	Late
Q777G6	*BFRF2*	15.326924	2.695240	Late
Q777G7	*BFRF1*	13.977429	4.110874	Late
Q777F4	*BSRF1*	11.033660	2.135708	Late
P03198	*BALF5*	10.829610	2.652654	Late
P03188	*BALF4*	10.288865	2.263927	Late
Q777A8	*BALF3*	10.272609	1.482687	Late
P03196	*BLRF1*	9.776421	0	Late
Q777A6	*BALF1*	9.347705	0	Late
P03212	*BKRF2*	9.008113	0	Late
Q777G9	*BFLF2*	7.946392	0	Late
P03197	*BLRF2*	7.040368	3.167441	Late
P03210	*BRRF2*	2.744946	1.495854	Late
P03234	*BVRF2*	1.927980	1.970797	Late
P03213	*BBRF1*	1.900693	1.295324	Late
Q777F0	*BLLF1*	1.562926	0.426489	Late
P03205	*BZLF2*	1.531303	14.527452	Late
P03226	*BcLF1*	1.007264	1.164494	Late
P03215	*BBRF3*	0.751845	0	Late
P03186	*BPLF1*	0.433027	1.419978	Late
P03180	*BCRF1*	0	2.962960	Late
Q777C5	*BDLF3*	0	1.953869	Late
P03189	*BOLF1*	0	1.846761	Late

[a] Read counts for each gene in the sample utilized for RNA-Seq analysis.

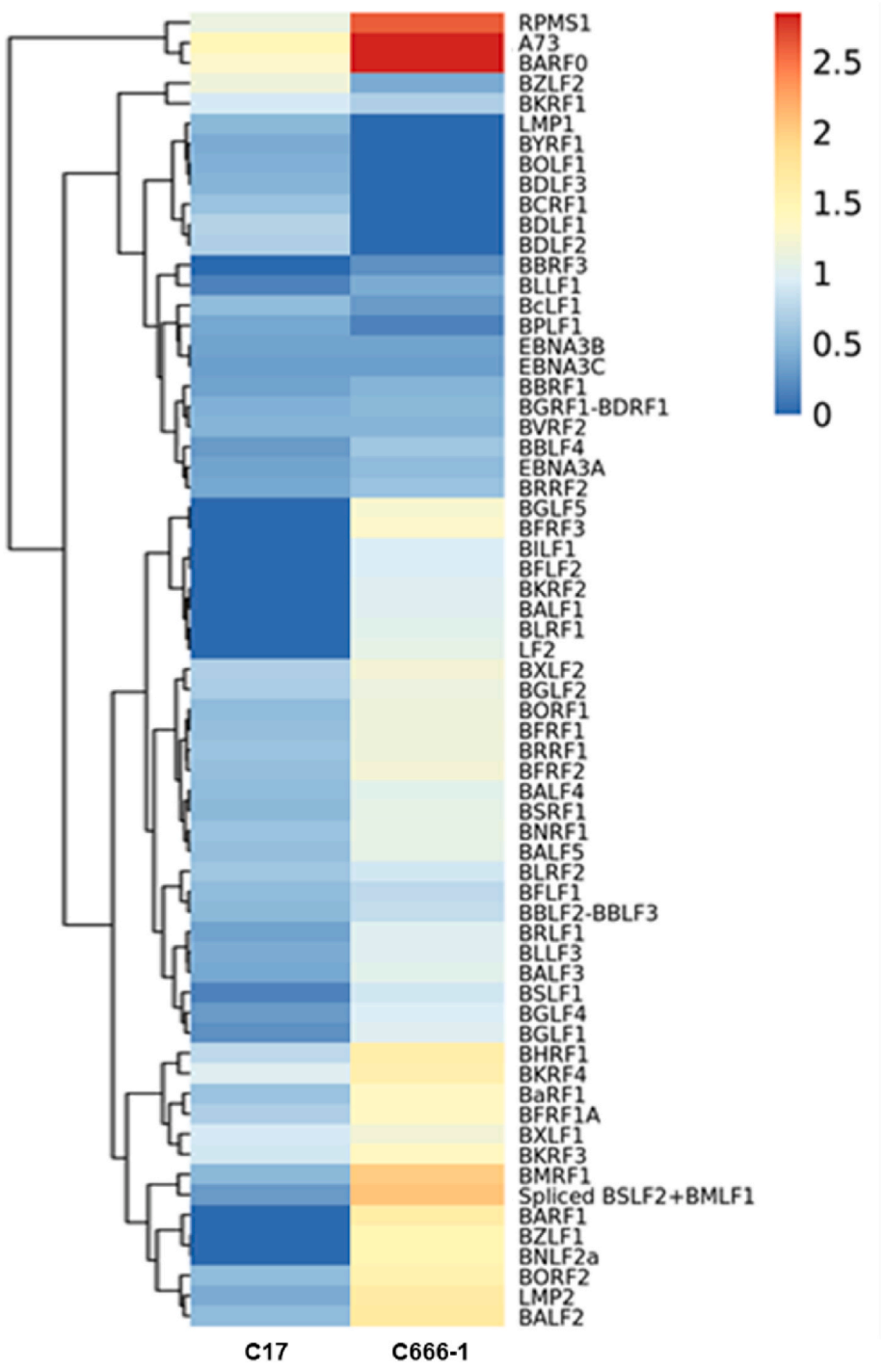

Fig. 10. Heatmap of EBV-genes found in C17 and C666-1 cell lines through RNA-Seq analysis (see also Table 5). The samples are displayed in columns and genes in rows. Dendrogram trees illustrate the clustering of both samples and genes. Samples or genes with comparable expression levels are clustered together with fewer branch points in the dendrogram. The color code represents the expression levels of individual genes in either C17 or C666-1 cells, with blue indicating low expression and red indicating high expression. (For interpretation of the references to color in this figure legend, the reader is referred to the Web version of this article.)

BBLF4 (helicase), and *BBLF2/3* (helicase-primase complex). *BZLF1*, but not *BRLF1*, binds to the oriLyt (lytic origin of DNA replication) and initiates EBV DNA replication while also transactivating methylated promoters. Although a complete lytic cycle requires a methylated viral genome, *BZLF1* can still induce the expression of early genes [67]. In EBV-positive cell lines, a subset of the cell population undergoes lytic infection. This means that among the cells carrying EBV, some will enter a phase where the virus replicates and generates new viral particles. This lytic phase can result in the destruction of the host cells as the new virus particles are released [68]. However, it is not commonly mentioned that C666–1 and C17 cells produce infectious EBV [23,34]. They are primarily used to study viral-host interactions involving EBV and nasopharyngeal carcinoma. Instead, these cells consistently contain a latent form of the EBV genome [69]. Taken together, the absence of *BZLF1* in the C17 cell line may influence the functional implications of EBV lytic gene expression in the oncogenic process. Traditionally, viral tumors

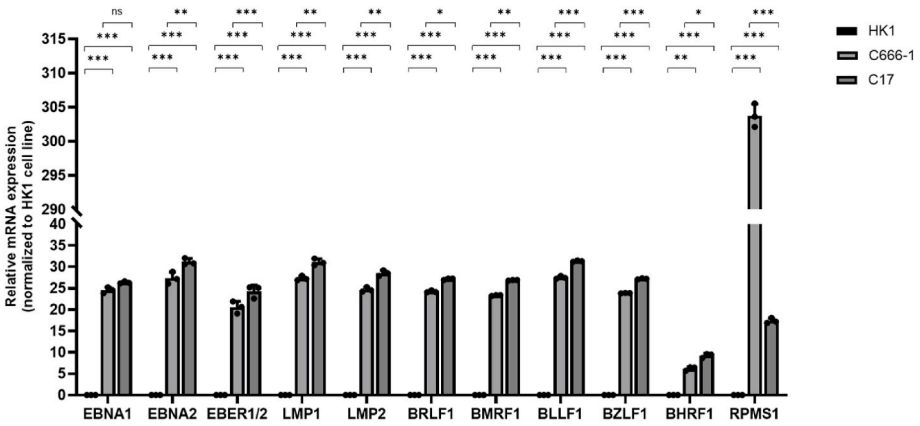

Fig. 11. Gene expression analysis in the HK1, C666-1, and C17 cell lines. RT-qPCR was used to assess the expression of EBV genes linked to type II latency and lytic EBV genes unique to NPC in the C666–1 and C17 cell lines. The expression levels were normalized to the gene expression of the EBV-negative cell line (HK1). To provide a more accurate representation of gene expression in other samples, the normalization value was set to 1. The data is presented as mean ± SD (n = 3 independent assays). Asterisks denote statistically significant differences between the two cell lines (**$p < 0.01$; ***$p < 0.001$).

Table 6
Expression of genes related to immune escape mechanisms in C666–1 and C17 cells.

Gene_ID	Gene_Name	C17[a]	C666-1[a]
ENSG00000120217.14	*PD-L1*	47.12	70.18
ENSG00000197646.8	*PD-L2*	36.41	0.88
ENSG00000121594.12	*CD80*	4.28	115.80
ENSG00000114013.16	*CD86*	9.64	16.67
ENSG00000168961.17	*Galectin-9*	297.74	116.68
ENSG00000189403.15	*HMGB1*	1974.93	3334.54
ENSG00000079385.23	*CEACAM1*	79.25	324.59
ENSG00000130202.10	*NECTIN2*	461.60	537.77
ENSG00000073008.16	*PVR*	434.83	1029.93
ENSG00000206503.14	*HLA-A*	7780.83	5106.65
ENSG00000234745.14	*HLA-B*	5821.96	8821.05
ENSG00000204525.18	*HLA-C*	2626.10	3874.95
ENSG00000204642.14	*HLA-F*	610.47	614.97
ENSG00000204632.13	*HLA-G*	87.82	4.39
ENSG00000204287.14	*HLA-DRA*	9869.28	11063.38
ENSG00000196126.12	*HLA-DRB1*	3286.90	5144.37
ENSG00000198502.6	*HLA-DRB5*	1046.37	283.36
ENSG00000290878.1	*HLA-DRB6*	172.43	182.47
ENSG00000179344.17	*HLA-DQB1*	682.23	350.91
ENSG00000196735.13	*HLA-DQA1*	1498.33	2257.24
ENSG00000204257.15	*HLA-DMA*	284.89	346.53
ENSG00000242574.9	*HLA-DMB*	356.64	377.23
ENSG00000204592.9	*HLA-E*	2090.59	1693.15
ENSG00000125657.5	*TNFSF9*	121.02	309.68
ENSG00000103855.18	*CD276*	1087.07	707.09

[a] Read counts for each gene in the sample utilized for RNA-Seq analysis.

were believed to be mainly caused by the latent phase of oncogenic viruses, as cells are typically lysed and killed during the lytic phase. However, there is growing evidence that the lytic life cycle of certain oncogenic viruses contributes to tumorigenesis [70–72]. For example, in the case of EBV, activation of the lytic cycle in nasopharyngeal carcinoma (NPC) can facilitate tumor progression. It has been found that the EBV lytic cycle in advanced NPC stages enhances the recruitment and differentiation of monocytes into tumor-associated macrophages (TAMs), which, in turn, support angiogenesis, invasion, and migration of the tumor [73,74]. Data suggests that similar mechanisms exist in other tumors, as well. Epigenetic modifications, such as histone deacetylase inhibitors, can promote the reactivation of viral lytic cycles, leading to the involvement of latent viruses in tumorigenesis.

Although both cell lines contain high levels of EBV DNA [24,75], and we were able to detect the expression of both latent and lytic EBV genes using RNA-Seq and PCR, we did not observe the production of infectious viral particles in the cells. While this phenomenon has been reported several times in both cell lines, it has not yet been thoroughly investigated or characterized. Therefore, here, we can only propose potential mechanisms that may contribute to the defect in the production of infectious EBV particles. One of the key factors contributing to the lack of infectious EBV particle production in C666–1 and C17 cells is the epigenetic regulation of the viral genome. In these cells, the EBV genome exists in an episomal, circularized form and is tightly associated with host histones, forming chromatin-like structures. This chromatinization leads to the silencing of the majority of EBV genes, particularly those involved in the lytic cycle, thereby maintaining the virus in a latent state. Epigenetic modifications such as DNA methylation and histone deacetylation further reinforce this transcriptional repression. As a result, even though lytic gene transcripts can occasionally be detected, the full reactivation of the lytic cycle and subsequent production of infectious viral particles is effectively blocked [76]. Histone modifications represent an additional potential mechanism contributing to the absence of infectious EBV particles. Proteins such as SFPQ (splicing factor proline and glutamine rich) play a role in maintaining EBV latency by promoting the expression of histone H1, which stabilizes nucleosomes and regulates nuclear architecture. This prevents the full activation of the lytic cycle. Histone H1 plays a crucial role in regulating EBV latency, functioning as a dynamic epigenetic regulator. Unlike core histones, H1 binds less tightly to DNA, allowing for rapid association and dissociation. Its levels fluctuate with cell differentiation, a key factor in EBV lytic reactivation. Changes in H1 abundance might signal shifts in chromatin structure, influencing viral genome accessibility and triggering immediate early gene expression. Additionally, repressive epigenetic marks—such as H3K9me3 and H3K27me3—stabilize latency but are removed during reactivation, prompting H1 unloading and degradation. This process likely contributes to the decline of H1.2 and H1.4 after lytic induction [77]. EBV expresses a diverse array of viral noncoding RNAs (ncRNAs) during latent infection, many of which possess regulatory functions that can modulate viral and host gene expression at the post-transcriptional level. Among the most well-characterized are the EBV-encoded RNAs (EBERs), *Bam*HI-A rightward transcripts (BARTs), a small nucleolar RNA (snoRNA), and a broad set of viral microRNAs (miRNAs), all of which are expressed across various EBV-infected cell types and associated malignancies. Recent studies have also uncovered additional novel ncRNAs encoded by EBV which are integral to key biological pathways. The regulatory activity of these ncRNAs may play a role in suppressing the lytic cycle and thereby limiting the production of infectious viral particles. By downregulating the expression of essential lytic genes or modulating host pathways that support viral replication, EBV ncRNAs may contribute to the observed deficiency in infectious virus production during latent or abortive lytic infection [78].

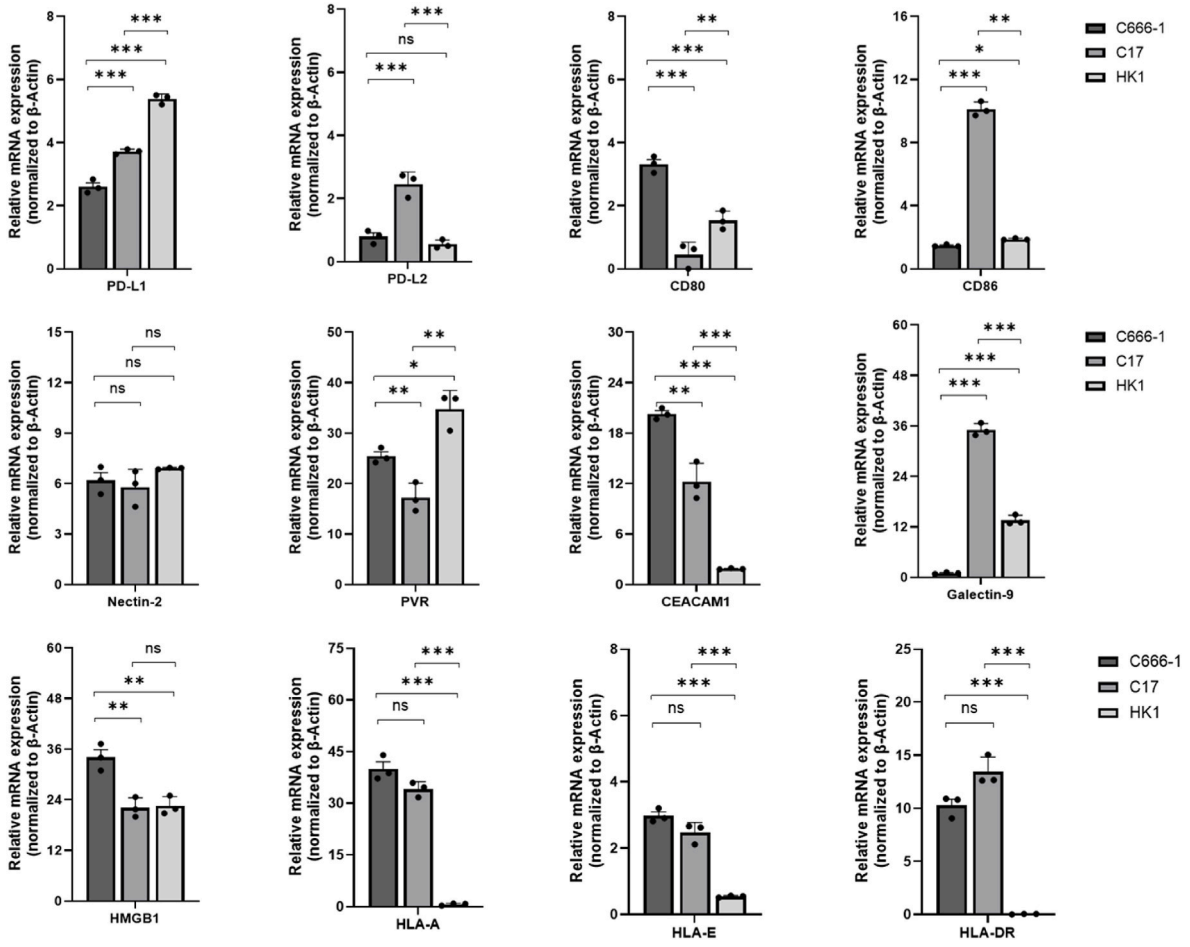

Fig. 12. Gene expression analysis in the HK1, C666-1, and C17 cell lines. RT-qPCR was used to assess the expression of genes related to immune escape mechanisms in the EBV positive cell lines: C666–1 and C17 and EBV negative cell line: HK1. The expression of the analyzed genes was normalized to β-actin expression. The data is presented as mean ± SD (n = 3 independent assays). Asterisks indicate statistically significant differences between the two cell lines (*$p < 0.05$; **$p < 0.01$; ***$p < 0.001$).

The HK1 cell line is widely recognized as a negative control for the detection of EBV-associated gene expression via RT-qPCR due to its EBV-negative status [79,80]. Derived from a nasopharyngeal carcinoma, the HK1 cell line lacks EBV, making it an ideal baseline for comparison against EBV-positive samples [49]. This characteristic ensures that any detected expression of EBV-associated genes in other samples is specifically due to the presence of EBV and not other factors. Our HK1 samples had a C_t value greater than 35 (data not shown), which, with 40 qPCR cycles, results in a negative outcome. A Ct value of 39 in qPCR indicates that the expression of the gene in question is very low, close to the detection limit of the assay. Typically, a C_t value over 35 is considered borderline for reliable detection. Therefore, while there is technically some expression, it is minimal and may not hold biological significance. This suggests that the specific gene was not expressed in our sample. Using HK1 as a negative control enhances the specificity and reliability of qPCR experiments by offering a consistent and well-documented reference point. This enables researchers to accurately distinguish between EBV-related gene expression and background noise, thereby improving the validity of their findings.

The somatic mutation rate in NPC is relatively low compared to other types of cancers [20], making it challenging to identify genes specific to NPC. Many genes identified in the literature are expressed not only in NPC but also in other carcinomas and healthy epithelial cells [53–56]. These genes, including *EpCAM, ERBB2, EGFR, ICAM1*, and *B7H3/CD276* serve as molecular biomarkers for understanding the pathogenesis of NPC and play roles in regulating morphology in normal healthy cells, stem/progenitor cells, and potentially driving tumor progression in cancer cells [81–92]. Our studies have shown that C666–1 and C17 cell lines express these genes, and are of great interest for the diagnosis and therapy of various cancers.

While we cannot definitively claim that these genes are specific to NPC, we believe they serve as reliable indicators of cellular activation in NPC. For example, *EpCAM* downregulates PTEN and activates AKT, mTOR, p70S6K, and 4EBP1, promoting NPC cell invasiveness [81,83,84,87,88]. *EGFR* overexpression in NPC is linked to poor survival due to ERK1/2 and AKT activation [89]. Elevated levels of circulating Intercellular Adhesion Molecule 1 (*ICAM-1*) have been observed in head and neck cancers, including NPC, suggesting a potential role in tumor progression and metastasis [59,89]. *B7H3/CD276*, upregulated in NPC, inhibits NK cell function via the PI3K/AKT/mTOR pathway activated by EBV *LMP1*. Targeting *B7H3/CD276* with PD-L1 blockade may restore NK cell activity [91]. *ERBB2/HER2* expression is higher in NPC tissues than in non-cancerous tissues, indicating potential therapeutic targeting [90].

Our study identified differential expression of certain genes between the C17 and C666-1 cell lines, highlighting their distinct molecular characteristics. Notably, *FGFR1, RET, GSTA3,* and *UCHL1* were found to be differentially expressed. *FGFR1*, which promotes NPC tumor progression and is associated with poor prognosis, is a potential therapeutic target [93]. The role of RET in NPC is not fully understood. However, RET can activate various downstream pathways, including PI3K/AKT, RAS/RAF/MEK/ERK, JAK2/STAT3, and PLCγ. This activation can lead

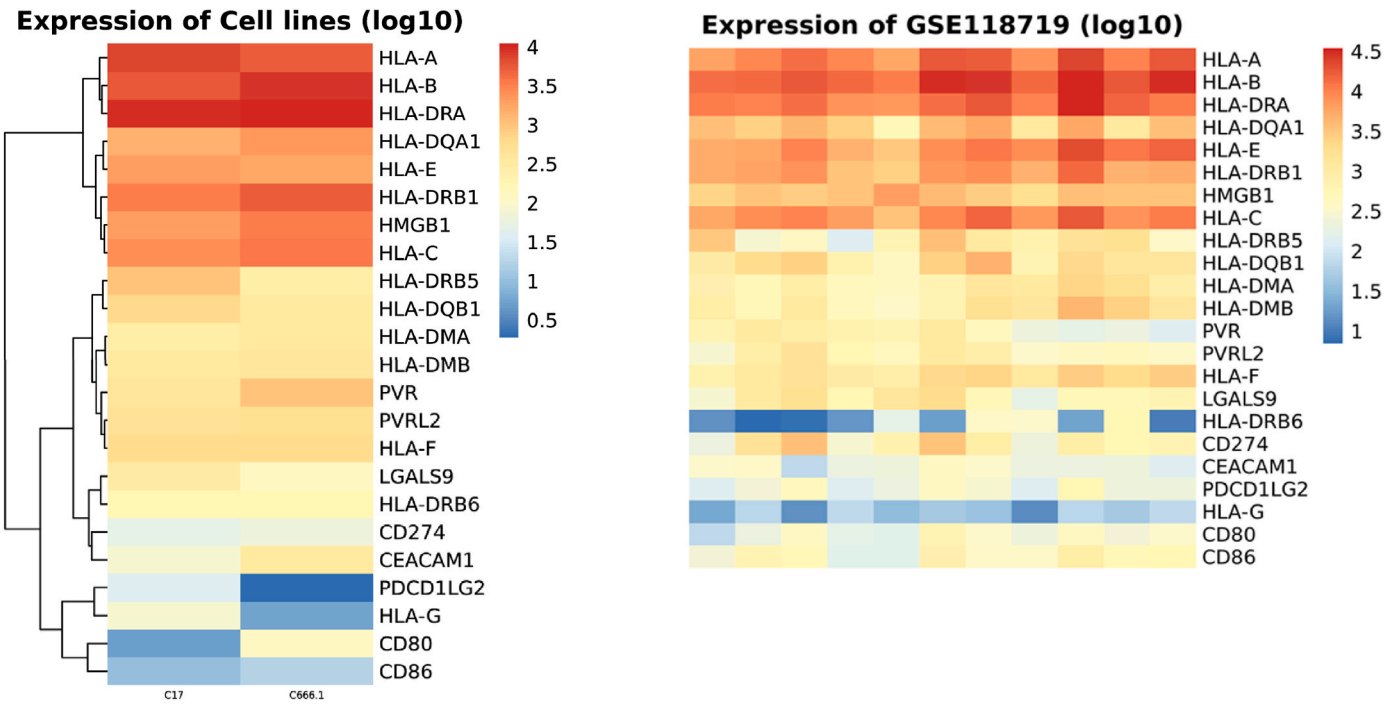

Fig. 13. Heatmap of genes related to immune escape mechanisms, identified in the C666–1 and C17 cell lines, as well as NPC tissue (GSE118719) (see also Suppl. Table 4 and Suppl Fig. 3). This comparison was performed using R 4.3. leveraging, the GEOquery package for data retrieval, and pheatmap for visualization. The columns represent samples, while the rows represent genes. Clustering of samples and genes is depicted by dendrogram trees. Samples or genes that are grouped closer together are illustrated with fewer branch points in the dendrogram. The color scheme indicates gene expression levels in either C17 or C666-1 cells, with blue indicating low expression, yellow indicating moderate expression, and red indicating high expression. (For interpretation of the references to color in this figure legend, the reader is referred to the Web version of this article.)

to increased cell proliferation, migration, survival, and differentiation, ultimately supporting neoplastic growth and tumorigenesis [94]. *GSTA3*, involved in detoxification processes, influences NPC susceptibility [95]. *UCHL1* functions as a tumor suppressor, with its downregulation being linked to metastasis [96]. Understanding the differential expression of these genes is crucial for developing tailored treatments for NPC.

5. Limitations and conclusions

While this *in vitro* RNA-seq study provides valuable insights into gene expression profiles, several limitations should be considered. In RNA-Seq analyses, certain transcripts can frequently be underrepresented due to biological factors. This could be the reason why some genes were not detected in the RNA-Seq analysis of C666-1 cells. One possible biological explanation could be the rapid degradation of LMP-1 mRNA or LMP-1 proteins, resulting in lower detectability in RNA-Seq analysis. However, RT-qPCR analyses are more sensitive and can detect even small amounts of transcripts, which may explain why LMP-1 is detected there. *In vitro* conditions may not fully replicate the complex *in vivo* environment, potentially affecting the relevance of the findings to physiological conditions. Additionally, the cell lines used may not capture the heterogeneity present in actual tissues, leading to an incomplete understanding of gene expression dynamics. Technical limitations such as sequencing depth and potential biases in library preparation can also impact the accuracy and reproducibility of the results.

In conclusion, our study highlights differences between C666–1 and C17 cell lines using bulk RNA-sequencing, emphasizing EBV gene expression patterns in NPC. The findings reveal distinct molecular characteristics and potential therapeutic targets, aiding in understanding NPC pathogenesis and the role of EBV in NPC and other EBV-associated carcinomas.

CRediT authorship contribution statement

Anna Makowska: Writing – review & editing, Writing – original draft, Visualization, Validation, Supervision, Project administration, Investigation, Funding acquisition, Formal analysis, Data curation. **Eva Miriam Buhl:** Investigation, Writing – review & editing. **Maximilian Göschel:** Writing – review & editing, Methodology, Investigation. **Chao-Chung Kuo:** Writing – review & editing, Validation, Methodology, Formal analysis. **Christina Nothbaum:** Writing – review & editing, Methodology, Investigation. **Emel Aylin Toktamis:** Investigation, Writing – review & editing. **Lian Shen:** Writing – review & editing, Methodology. **Ali T. Abdallah:** Methodology, Formal analysis. **Ralf Weiskirchen:** Writing – review & editing, Writing – original draft, Validation, Supervision, Resources, Project administration, Formal analysis, Conceptualization. **Udo Kontny:** Writing – review & editing, Supervision, Resources, Project administration, Funding acquisition.

Informed consent statement

Not applicable.

Institutional review board statement

Not applicable.

Data availability statement

The data presented in this study are available on request from the corresponding author.

Funding

This research has received no funding.

Declaration of competing interest

The authors declare no conflicts of interest.

Acknowledgments

The authors are grateful to Prof. Fei-Fei Liu (University of Toronto, Canada), Prof. Kwok Wai Lo (Chinese University of Hong Kong, China) and Prof. Sai Wah Tsao (Chinese University of Hong Kong, China) for providing NPC-cell lines for our study.

Abbreviations

DEG(s)	Differentially expressed gene(s)
EBV	Epstein-Barr virus
GSEA	Gene Set Enrichment Analysis
ICLAC	International Cell Line Authentication Committee
NPC	Nasopharyngeal carcinoma
RNA-Seq	RNA-sequencing
RT-qPCR	Quantitative real-time PCR

Appendix A. Supplementary data

Supplementary data to this article can be found online at https://doi.org/10.1016/j.bbrc.2025.152053.

References

[1] E.T. Chang, W. Ye, Y.X. Zeng, H.O. Adami, The evolving epidemiology of nasopharyngeal carcinoma, Cancer Epidemiol. Biomarkers Prev. 30 (6) (2021) 1035–1047, https://doi.org/10.1158/1055-9965.EPI-20-1702.

[2] Z.Y. Su, P.Y. Siak, Y.Y. Lwin, S.C. Cheah, Epidemiology of nasopharyngeal carcinoma: current insights and future outlook, Cancer Metastasis Rev. 43 (3) (2024) 919–939, https://doi.org/10.1007/s10555-024-10176-9.

[3] Y. Zhang, H. Rumgay, M. Li, S. Cao, W. Chen, Nasopharyngeal cancer incidence and mortality in 185 countries in 2020 and the projected burden in 2040: population-Based global epidemiological profiling, JMIR Public Health Surveill 9 (2023) e49968, https://doi.org/10.2196/49968.

[4] S. Lei, L. Chen, P. Ji, K. Li, Q. Li, C. Huang, G. Wang, J. Ma, R. Guo, L. Tang, Global burdens of nasopharyngeal carcinoma in children and young adults and predictions to 2040, Oral Oncol. 155 (2024) 106891, https://doi.org/10.1016/j.oraloncology.2024.106891.

[5] L. Zhang, Q.Y. Chen, H. Liu, L.Q. Tang, H.Q. Mai, Emerging treatment options for nasopharyngeal carcinoma, Drug Des. Dev. Ther. 7 (2013) 37–52, https://doi.org/10.2147/DDDT.S30753.

[6] S.I. Okekpa, R.B. Mydin, E. Mangantig, N.S.A. Azmi, S.N.S. Zahari, G. Kaur, Y. Musa, Nasopharyngeal carcinoma (NPC) risk factors: a systematic review and meta-analysis of the association with lifestyle, diets, socioeconomic and sociodemographic in Asian region, Asian Pac. J. Cancer Prev. APJCP 20 (11) (2019) 3505–3514, https://doi.org/10.31557/APJCP.2019.20.

[7] S.K. Yong, T.C. Ha, M.C. Yeo, V. Gaborieau, J.D. McKay, J. Wee, Associations of lifestyle and diet with the risk of nasopharyngeal carcinoma in Singapore: a case-control study, Chin. J. Cancer 36 (1) (2017) 3, https://doi.org/10.1186/s40880-016-0174-3.

[8] A. Hildesheim, C.P. Wang, Genetic predisposition factors and nasopharyngeal carcinoma risk: a review of epidemiological association studies, 2000–2011, Semin. Cancer Biol. 22 (2) (2012) 107–116, https://doi.org/10.1016/j.semcancer.2012.01.007.

[9] D.E. Spratt, N. Lee, Current and emerging treatment options for nasopharyngeal carcinoma, OncoTargets Ther. 5 (2012) 297–308, https://doi.org/10.2147/OTT.S28032.

[10] K. Liu, Y. Zhu, S. Li, H. Zhu, Chemoradiotherapy plus immunotherapy for locoregionally advanced nasopharyngeal carcinoma: a cost-effectiveness analysis, Head Neck (2024), https://doi.org/10.1002/hed.27932 (online ahead of print).

[11] A. Bongiovanni, A. Vagheggini, V. Fausti, L. Mercatali, S. Calpona, G. Di Menna, G. Miserocchi, T. Ibrahim, Induction chemotherapy plus concomitant chemoradiotherapy in nasopharyngeal carcinoma: an updated network meta-analysis, Crit. Rev. Oncol. Hematol. 160 (2021) 103244, https://doi.org/10.1016/j.critrevonc.2021.103244.

[12] T. Yoshizaki, A novel immune evasion mechanism of LMP-1, an EBV-Primary oncogene, in nasopharyngeal carcinoma, Adv. Otorhinolaryngol. 72 (2011) 157–159, https://doi.org/10.1159/000324780.

[13] S. Cheung, D. Huang, A. Hui, K. Lo, C. Ko, Y. Tsang, N. Wong, B. Whitney, J. Lee, Nasopharyngeal carcinoma cell line (C666–1) consistently harbouring epstein-barr virus, Int. J. Cancer 83 (1) (1999) 121–126, https://doi.org/10.1002/(sici)1097-0215(19990924)83:1<121::aid-ijc21>3.0.co;2-f.

[14] Z.Y. Su, P.Y. Siak, C.O. Leong, S.C. Cheah, The role of epstein-barr virus in nasopharyngeal carcinoma, Front. Microbiol. 14 (2023) 1116143, https://doi.org/10.3389/fmicb.2023.1116143.

[15] F. Petersson, Nasopharyngeal carcinoma: a review, Semin. Diagn. Pathol. 32 (1) (2015) 54–73, https://doi.org/10.1053/j.semdp.2015.02.021.

[16] B.B. Ma, A. King, Y.M. Lo, et al., Relationship between pretreatment level of plasma epstein-barr virus DNA, tumor burden, and metabolic activity in advanced nasopharyngeal carcinoma, Int. J. Radiat. Oncol. Biol. Phys. 66 (3) (2006) 714–720, https://doi.org/10.1016/j.ijrobp.2006.05.064.

[17] L.Q. Tang, C.F. Li, J. Li, et al., Establishment and validation of prognostic nomograms for endemic nasopharyngeal carci-noma, J Natl Cancer Inst 108 (1) (2015) djv291, https://doi.org/10.1093/jnci/djv291.

[18] W.Z. Li, H.J. Wu, S.H. Lv, X.F. Hu, H. Liang, G.Y. Liu, N. Lu, W.X. Bei, X. Lv, X. Guo, W.X. Xia, Y.Q. Xiang, Assessment of survival model performance following inclusion of epstein-barr virus DNA status in conventional TNM staging groups in epstein-barr virus-related nasopharyngeal carcinoma, JAMA Netw. Open 4 (9) (2021) e2124721, https://doi.org/10.1001/jamanetworkopen.2021.24721.

[19] J.A. Kanakry, A.M. Hegde, C.M. Durand, A.B. Massie, A.E. Greer, R.F. Ambinder, A. Valsamakis, The clinical significance of EBV DNA in the plasma and peripheral blood mononuclear cells of patients with or without EBV diseases, Blood 127 (16) (2016) 2007–2017, https://doi.org/10.1182/blood-2015-09-672030.

[20] J.I. Kawada, Y. Ito, K. Ohshima, M. Yamada, S. Kataoka, H. Muramatsu, A. Sawada, T. Wada, K.I. Imadome, A. Arai, K. Iwatsuki, S. Ohga, H. Kimura, Committee for guidelines for the management of chronic active EBV disease, related disorders (the MHLW research team in Japan). Updated guidelines for chronic active epstein-barr virus disease, Int. J. Hematol. 118 (5) (2023) 568–576, https://doi.org/10.1007/s12185-023-03660-5.

[21] P.M. Hau, H.L. Lung, M. Wu, C.M. Tsang, K.L. Wong, N.K. Mak, K.W. Lo, Targeting epstein-barr virus in nasopharyngeal carcinoma, Front. Oncol. 10 (2020) 600, https://doi.org/10.3389/fonc.2020.00600.

[22] ICLAC register of misidentified cell lines, Available at: https://iclac.org/databases/cross-contaminations/. (Accessed 11 December 2024).

[23] Y. Yip, W. Lin, W. Deng, L. Jia, K. Lo, P. Busson, B. Vérillaud, X. Liu, C. Tsang, M. Lung, S. Tsao, Establishment of a nasopharyngeal carcinoma cell line capable of undergoing lytic epstein-barr virus reactivation, Lab. Invest. 98 (8) (2018) 1093–1104, https://doi.org/10.1038/s41374-018-0034-7.

[24] Makowska A, Kontny U, van Helden J, Hildebrandt B, Schüler HM, Weiskirchen R. Genetic characterization of the immortalized human nasopharyngeal carcinoma cell line NPC/HK1. Cancer Med., doi: 10.1002/cam4.70422. ePub ahead of print.

[25] M.J. Strong, M. Baddoo, A. Nanbo, M. Xu, A. Puetter, Z. Lin, Comprehensive high-throughput RNA sequencing analysis reveals contamination of multiple nasopharyngeal carcinoma cell lines with HeLa cell genomes, J. Virol. 88 (18) (2014) 10696–10704, https://doi.org/10.1128/JVI.01457-14.

[26] S.Y. Chan, K.W. Choy, S.W. Tsao, Q. Tao, T. Tang, G.T. Chung, K.W. Lo, Authentication of nasopharyngeal carcinoma tumor lines, Int. J. Cancer 122 (2008) 2169–2171, https://doi.org/10.1002/ijc.23374.

[27] F. Ye, C. Chen, J. Qin, J. Liu, C. Zheng, Genetic profiling reveals an alarming rate of cross-contamination among human cell lines used in China, FASEB J. 29 (2015) 4268–4272, https://doi.org/10.1096/fj.14-266718.

[28] J.L. Almeida, C.T. Korch, Authentication of human and mouse cell lines by short tandem repeat (STR) DNA genotype analysis. 2023 Jan 17, in: S. Markossian, A. Grossman, M. Arkin, D. Auld, C. Austin, J. Baell, K. Brimacombe, T.D.Y. Chung, N.P. Coussens, J.L. Dahlin, V. Devanarayan, T.L. Foley, M. Glicksman, K. Gorshkov, J.V. Haas, M.D. Hall, S. Hoare, J. Inglese, P.W. Iversen, M. Lal-Nag, Z. Li, J. R. Manro, J. McGee, O. McManus, M. Pearson, T. Riss, P. Saradjian, G. S. Sittampalam, M. Tarselli, O.J. Trask, J.R. Weidner, M.J. Wildey, K. Wilson, M. Xia, X. Xu (Eds.), Assay Guidance Manual [Internet], Eli Lilly & Company and the National Center for Advancing Translational Sciences, Bethesda (MD), 2004. PMID: 23805434.

[29] P.A. Ewels, A. Peltzer, S. Fillinger, H. Patel, J. Alneberg, A. Wilm, M.U. Garcia, P. Di Tommaso, S. Nahnsen, The nf-core framework for community-curated bioinformatics pipelines, Nat. Biotechnol. 38 (3) (2020) 276–278, https://doi.org/10.1038/s41587-020-0439-x.

[30] P. Di Tommaso, M. Chatzou, E.W. Floden, P.P. Barja, E. Palumbo, C. Notredame, Nextflow enables reproducible computational workflows, Nat. Biotechnol. 35 (4) (2017 11) 316–319, https://doi.org/10.1038/nbt.3820.

[31] L. Li, Q. Tao, H. Jin, A. van Hasselt, F.F. Poon, X. Wang, M.S. Zeng, W.H. Jia, Y. Zeng, A. Chan, Y. Cao, The tumor suppressor UCHL1 forms a complex with p53/MDM2/ARF to promote p53 signaling and is frequently silenced in nasopharyngeal carcinoma, Clin. Cancer Res. 16 (11) (2010) 2949–2958, https://doi.org/10.1158/1078-0432.CCR-09-3178.

[32] K. Meganathan, S. Jagtap, V. Wagh, J. Winkler, J.A. Gaspar, D. Hildebrand, M. Trusch, K. Lehmann, J. Hescheler, H. Schlüter, A. Sachinidis, Identification of thalidomide-specific transcriptomics and proteomics signatures during differentiation of human embryonic stem cells, PLoS One 7 (8) (2012) e44228, https://doi.org/10.1371/journal.pone.0044228.

[33] E.G. Halakos, A.J. Connell, L. Glazewski, S. Wei, R.W. Mason, Bottom up proteomics identifies neuronal differentiation pathway networks activated by cathepsin inhibition treatment in neuroblastoma cells that are enhanced by concurrent 13-cis retinoic acid treatment, J Proteomics 232 (2021) 104068, https://doi.org/10.1016/j.jprot.2020.104068.

[34] P. Castillo, O. Aisagbonhi, C.C. Saenz, W.M. ElShamy, Novel insights linking BRCA1-IRIS role in mammary gland development to formation of aggressive PABCs: the case for longer breastfeeding, Am. J. Cancer Res. 12 (1) (2022) 396–426. PMID: 35141026.

[35] A.W.Y. Chai, S.M. Yee, H.M. Lee, N. Abdul Aziz, P.S. Yee, M. Marzuki, K.W. Wong, A.K.S. Chiang, L.K. Chow, W. Dai, T.F. Liu, L.P. Tan, A.S.B. Khoo, K.W. Lo, P.V. H. Lim, P. Rajadurai, H. Lightfoot, S. Barthorpe, M.J. Garnett, S.C. Cheong, Establishment and characterization of an epstein-barr virus-positive cell line from a non-keratinizing differentiated primary nasopharyngeal carcinoma, Cancer Res. Commun. 4 (3) (2024) 645–659, https://doi.org/10.1158/2767-9764.CRC-23-0341.

[36] M.K. Janani, J. Malathi, J. Biswas, S. Sridharan, H.N. Madhavan, Genotypic detection of epstein barr virus from clinically suspected viral retinitis patients in a tertiary eye care centre, India, Ocul. Immunol. Inflamm. 23 (5) (2015) 384–391, https://doi.org/10.3109/09273948.2014.968265.

[37] L. Glover, mSphere of influence: expanding the CRISPR sphere with single-locus proteomics, mSphere 5 (1) (2020), https://doi.org/10.1128/mSphere.00001-20.

[38] B. Melichar, M.A. Nash, R. Lenzi, C.D. Platsoucas, R.S. Freedman, Expression of costimulatory molecules CD80 and CD86 and their receptors CD28, CTLA-4 on malignant ascites CD3+ tumour-infiltrating lymphocytes (TIL) from patients with ovarian and other types of peritoneal carcinomatosis, Clin. Exp. Immunol. 119 (1) (2000) 19–27, https://doi.org/10.1046/j.1365-2249.2000.01105.x.

[39] W. Yang, P.W. Chen, H. Li, H. Alizadeh, J.Y. Niederkorn, PD-L1: PD-1 interaction contributes to the functional suppression of T-cell responses to human uveal melanoma cells in vitro, Investig. Ophthalmol. Vis. Sci. 49 (6) (2008) 2518–2525, https://doi.org/10.1167/iovs.07-1606.

[40] S.S. Hassan, M. Akram, E.C. King, H.M. Dockrell, J.M. Cliff, PD-1, PD-L1 and PD-L2 gene expression on T-cells and natural killer cells declines in conjunction with a reduction in PD-1 protein during the intensive phase of tuberculosis treatment, PLoS One 10 (9) (2015) e0137646, https://doi.org/10.1371/journal.pone.0137646.

[41] K.J. Dery, C. Silver, L. Yang, J.E. Shively, Interferon regulatory factor 1 and a variant of heterogeneous nuclear ribonucleoprotein L coordinately silence the gene for adhesion protein CEACAM1, J. Biol. Chem. 293 (24) (2018) 9277–9291, https://doi.org/10.1074/jbc.RA117.

[42] C.X. Zhang, D.J. Huang, V. Baloche, L. Zhang, J.X. Xu, B.W. Li, X.R. Zhao, J. He, H. Q. Mai, Q.Y. Chen, X.S. Zhang, P. Busson, J. Cui, J. Li, Galectin-9 promotes a suppressive microenvironment in human cancer by enhancing STING degradation, Oncogenesis 9 (7) (2020) 65, https://doi.org/10.1038/s41389-020-00248-0.

[43] V. Kruse, C. Hamann, S. Monecke, L. Cyganek, L. Elsner, D. Hübscher, L. Walter, K. Streckfuss-Bömeke, K. Guan, R. Dressel, Human induced pluripotent stem cells are targets for allogeneic and autologous natural killer (NK) cells and killing is partly mediated by the activating NK receptor DNAM-1, PLoS One 10 (5) (2015) e0125544, https://doi.org/10.1371/journal.pone.0125544.

[44] B. Seliger, S. Jasinski-Bergner, D. Quandt, C. Stoehr, J. Bukur, S. Wach, W. Legal, H. Taubert, B. Wullich, A. Hartmann, HLA-E expression and its clinical relevance in human renal cell carcinoma, Oncotarget 7 (41) (2016) 67360–67372, https://doi.org/10.18632/oncotarget.11744.

[45] A. Maenaka, I. Kenta, A. Ota, Y. Miwa, W. Ohashi, K. Horimi, Y. Matsuoka, M. Ohnishi, K. Uchida, T. Kobayashi, Interferon-γ-induced HLA class II expression on endothelial cells is decreased by inhibition of mTOR and HMG-CoA reductase, FEBS Open Bio 10 (5) (2020) 927–936, https://doi.org/10.1002/2211-5463.12854.

[46] S. Kawashima, T. Inozume, M. Kawazu, T. Ueno, J. Nagasaki, E. Tanji, A. Honobe, T. Ohnuma, T. Kawamura, Y. Umeda, Y. Nakamura, T. Kawasaki, Y. Kiniwa, O. Yamasaki, S. Fukushima, Y. Ikehara, H. Mano, Y. Suzuki, H. Nishikawa, H. Matsue, Y. Togashi, TIGIT/CD155 axis mediates resistance to immunotherapy in patients with melanoma with the inflamed tumor microenvironment, J. Immunother. Cancer 9 (11) (2021) e003134, https://doi.org/10.1136/jitc-2021-003134.

[47] Y.D. Dong, L. Cui, C.H. Peng, D.F. Cheng, B.S. Han, F. Huang, Expression and clinical significance of HMGB1 in human liver cancer: knockdown inhibits tumor growth and metastasis in vitro and in vivo, Oncol. Rep. 29 (1) (2013) 87–94, https://doi.org/10.3892/or.2012.2070.

[48] The cellosaurus STR similarity search tool CLASTR 1.4.4, Available at: https://www.cellosaurus.org/str-search/. (Accessed 11 December 2024).

[49] A. Bairoch, The cellosaurus, a cell-line knowledge resource, J. Biomol. Tech. 29 (2) (2018) 25–38, https://doi.org/10.7171/jbt.18-2902-002.

[50] J.L. Almeida, A. Dakic, K. Kindig, M. Kone, D.L.D. Letham, S. Langdon, R. Peat, J. Holding-Pillai, E.M. Hall, M. Ladd, M.D. Shaffer, H. Berg, J. Li, G. Wigger, S. Lund, C.R. Steffen, B.B. Fransway, B. Geraghty, M. Natoli, B. Bauer, S.M. Gollin, D.W. Lewis, Y. Reid, Interlaboratory study to validate a STR profiling method for intraspecies identification of mouse cell lines, PLoS One 14 (6) (2019) e0218412, https://doi.org/10.1371/journal.pone.0218412.

[51] S.Y. Chan, K.W. Choy, S.W. Tsao, Q. Tao, T. Tang, G.T. Chung, K.W. Lo, Authentication of nasopharyngeal carcinoma tumor lines, Int. J. Cancer 122 (9) (2008) 2169–2171, https://doi.org/10.1002/ijc.23374.

[52] F. Ye, C. Chen, J. Qin, J. Liu, C. Zheng, Genetic profiling reveals an alarming rate of cross-contamination among human cell lines used in China, FASEB J. 29 (10) (2015) 4268–4272, https://doi.org/10.1096/fj.14-266718.

[53] W. Lin, Y.L. Yip, L. Jia, W. Deng, H. Zheng, W. Dai, J.M.Y. Ko, K.W. Lo, G.T. Y. Chung, K.Y. Yip, S.D. Lee, J.S. Kwan, J. Zhang, T. Liu, J.Y. Chan, D.L. Kwong, V. H. Lee, J.M. Nicholls, P. Busson, X. Liu, A.K.S. Chiang, K.F. Hui, H. Kwok, S. T. Cheung, Y.C. Cheung, C.K. Chan, B. Li, A.L. Cheung, P.M. Hau, Y. Zhou, C. M. Tsang, J. Middeldorp, H. Chen, M.L. Lung, S.W. Tsao, Establishment and characterization of new tumor xenografts and cancer cell lines from EBV-Positive nasopharyngeal carcinoma, Nat. Commun. 9 (1) (2018) 4663, https://doi.org/10.1038/s41467-018-06889-5.

[54] W. Dai, H. Zheng, A.K. Cheung, M.L. Lung, Genetic and epigenetic landscape of nasopharyngeal carcinoma, Chin. Clin. Oncol. 5 (2) (2016) 16, https://doi.org/10.21037/cco.2016.03.06.

[55] Y. Wang, M. Li, Y. Guo, H. Huang, X. Dong, Y. Sun, J. Liu, Key genes affecting the progression of nasopharyngeal carcinoma identified by RNA-Sequencing and bioinformatic analysis, Aging (Albany NY) 13 (18) (2021) 22176–22187, https://doi.org/10.18632/aging.203521.

[56] L. Gong, D.L. Kwong, W. Dai, P. Wu, S. Li, Q. Yan, Y. Zhang, B. Zhang, X. Fang, L. Liu, M. Luo, B. Liu, L.K. Chow, Q. Chen, J. Huang, V.H. Lee, K.O. Lam, A.W. Lo, Z. Chen, Y. Wang, A.W. Lee, X.Y. Guan, Comprehensive single-cell sequencing reveals the stromal dynamics and tumor-specific characteristics in the microenvironment of nasopharyngeal carcinoma, Nat. Commun. 12 (1) (2021) 1540, https://doi.org/10.1038/s41467-021-21795-z.

[57] Z.C. Zhang, S. Fu, F. Wang, H.Y. Wang, Y.X. Zeng, J.Y. Shao, Oncogene mutational profile in nasopharyngeal carcinoma, OncoTargets Ther. 7 (2014) 457–467, https://doi.org/10.2147/OTT.S58791.

[58] C. Fan, J. Wang, Y. Tang, S. Zhang, F. Xiong, C. Guo, Y. Zhou, Z. Li, X. Li, Y. Li, G. Li, Z. Zeng, W. Xiong, Upregulation of long non-coding RNA LOC284454 May serve as a new serum diagnostic biomarker for head and neck cancers, BMC Cancer 20 (1) (2020) 917, https://doi.org/10.1186/s12885-020-07408-w.

[59] T. Murata, Encyclopedia of EBV-Encoded lytic genes: an update, in: Y. Kawaguchi, Y. Mori, H. Kimura (Eds.), Human Herpesviruses, Advances in Experimental Medicine and Biology, vol.1045, Springer, Singapore, 2018, https://doi.org/10.1007/978-981-10-7230-7_18.

[60] Y. Zeng, C.L. Luo, G.W. Lin, F. Li, X. Bai, J.M. Ko, L. Xiong, Y. Liu, S. He, J.X. Jiang, W.X. Yan, E.H.W. Ong, Z. Li, Y.Q. Zhou, Y.H. Zhou, A.Y. Xu, S.Q. Liu, Y.M. Guo, J. R. Chen, X.X. Cheng, Y.L. Cao, X. Yu, B. Wu, P.P. Wei, Z.H. Ruan, Q.Y. Chen, L. Q. Tang, J.D. McKay, W.H. Jia, H.Q. Mai, S.T. Lim, J.J. Liu, D.X. Lin, C.C. Khor, M. L.K. Chua, M. Ji, M.L. Lung, Y.X. Zeng, J.X. Bei, Whole-exome sequencing association study reveals genetic effects on tumor microenvironment components in nasopharyngeal carcinoma, J. Clin. Investig. 135 (1) (2025) e182768, https://doi.org/10.1172/JCI182768.

[61] C. Lin, J. Zong, W. Lin, M. Wang, Y. Xu, R. Zhou, S. Lin, Q. Guo, H. Chen, Y. Ye, B. Zhang, J. Pan, EBV-miR-BART8-3p induces epithelial-mesenchymal transition and promotes metastasis of nasopharyngeal carcinoma cells through activating NF-κB and Erk1/2 pathways, J. Exp. Clin. Cancer Res. 37 (1) (2018) 283, https://doi.org/10.1186/s13046-018-0953-6.

[62] J.M. Silva, C.E.C. Alves, G.S. Pontes, Epstein-barr virus: the mastermind of immune chaos, Front. Immunol. 15 (2024) 1297994, https://doi.org/10.3389/fimmu.2024.1297994.

[63] S.W. Tsao, C.M. Tsang, K.F. To, K.W. Lo, The role of epstein-barr virus in epithelial malignancies, J. Pathol. 235 (2) (2015) 323–333, https://doi.org/10.1002/path.4448.

[64] A. Molina-Herrera, K. Rubio, S.A. Benavides-Suárez, M.E. Torres-García, Epstein-barr virus: a novel dimension in cancer development, in: N. Velázquez-Márquez, G. A. Paredes-Juárez, V. Vallejo-Ruiz (Eds.), Pathogens Associated with the Development of Cancer in Humans, Springer, Cham, 2024, https://doi.org/10.1007/978-3-031-62558-9_6.

[65] A. El-Sharkawy, L. Al Zaidan, A. Malki, Epstein-barr virus-associated malignancies: roles of viral oncoproteins in carcinogenesis, Front. Oncol. 8 (2018) 265, https://doi.org/10.3389/fonc.2018.00265.

[66] L. Hu, Z. Lin, Y. Wu, J. Dong, B. Zhao, Y. Cheng, P. Huang, L. Xu, T. Xia, D. Xiong, H. Wang, M. Li, L. Guo, E. Kieff, Y. Zeng, Q. Zhong, M. Zeng, Comprehensive profiling of EBV gene expression in nasopharyngeal carcinoma through paired-end transcriptome sequencing, Front. Med. 10 (1) (2016) 61–75, https://doi.org/10.1007/s11684-016-0436-0.

[67] L.F. Yap, A.K.C. Wong, I.C. Paterson, L.S. Young, Functional implications of epstein-barr virus lytic genes in carcinogenesis, Cancers (Basel) 14 (23) (2022) 5780, https://doi.org/10.3390/cancers14235780.

[68] B. Damania, S.C. Kenney, N. Raab-Traub, Epstein-barr virus: biology and clinical disease, Cell 185 (20) (2022) 3652–3670, https://doi.org/10.1016/j.cell.2022.08.026.

[69] K.K. Tso, K.Y. Yip, C.K. Mak, G.T. Chung, S.D. Lee, S.T. Cheung, K.F. To, K.W. Lo, Complete genomic sequence of epstein-barr virus in nasopharyngeal carcinoma cell line C666-1, Infect Agent Cancer 8 (1) (2013) 29, https://doi.org/10.1186/1750-9378-8-29.

[70] Q. Rosemarie, B. Sugden, Epstein-barr virus: how its lytic phase contributes to oncogenesis, Microorganisms 8 (11) (2020) 1824, https://doi.org/10.3390/microorganisms8111824.

[71] Y. Deng, C. Münz, Roles of lytic viral replication and co-infections in the oncogenesis and immune control of the epstein-barr virus, Cancers (Basel) 13 (9) (2021) 2275, https://doi.org/10.3390/cancers13092275.

[72] M. Dorothea, J. Xie, S.P.T. Yiu, A.K.S. Chiang, Contribution of epstein-barr virus lytic proteins to cancer hallmarks and implications from other oncoviruses, Cancers (Basel) 15 (7) (2023) 2120, https://doi.org/10.3390/cancers15072120.

[73] X. Xu, N. Zhu, J. Zheng, Y. Peng, M.S. Zeng, K. Deng, C. Duan, Y. Yuan, EBV abortive lytic cycle promotes nasopharyngeal carcinoma progression through recruiting monocytes and regulating their directed differentiation, PLoS Pathog. 20 (1) (2024) e1011934, https://doi.org/10.1371/journal.ppat.1011934.

[74] S. Lin, H. Zhou, G. Chen, J. Xue, Q. Liu, J. Li, Y. Yang, Y. Zhao, H. Bao, Y. Huang, Y. Ma, H. Zhao, Early change of plasma epstein-barr virus DNA load and the viral lytic genome level could positively predict clinical outcome in recurrent or metastatic nasopharyngeal carcinoma receiving anti-programmed cell death 1 monotherapy, BMC Cancer 24 (1) (2024) 797, https://doi.org/10.1186/s12885-024-12564-4.

[75] X. Wang, L. Yu, X. Zhou, A.M.T. Liu, Y.Y. Chan, M. Wu, K.Y. Chau, K.W. Lo, A. R. Wuet, Characterizing resistant cellular states in nasopharyngeal carcinoma during EBV lytic induction, Oncogene (2025), https://doi.org/10.1038/s41388-025-03341-z.
[76] A.S. Torne, E.S. Robertson, Epigenetic mechanisms in latent epstein-barr virus infection and associated cancers, Cancers (Basel) 16 (5) (2024) 991, https://doi.org/10.3390/cancers16050991.
[77] L.A. Murray-Nerger, C. Lozano, E.M. Burton, et al., The nucleic acid binding protein SFPQ represses EBV lytic reactivation by promoting histone H1 expression, Nat. Commun. 15 (2024) 4156, https://doi.org/10.1038/s41467-024-48333-x.
[78] R.L. Skalsky, B.R. Cullen, EBV noncoding RNAs, Curr. Top. Microbiol. Immunol. 391 (2015) 181–217, https://doi.org/10.1007/978-3-319-22834-1_6.
[79] M. Abou Harb, DG Jr Meckes, L. Sun, Epstein-barr virus LMP1 enhances levels of large ex-tracellular vesicle-associated PD-L1, J. Virol. 97 (10) (2023) e0021923, https://doi.org/10.1128/jvi.00219-23.
[80] J. Ge, J. Wang, F. Xiong, X. Jiang, K. Zhu, Y. Wang, Y. Mo, Z. Gong, S. Zhang, Y. He, X. Li, L. Shi, C. Guo, F. Wang, M. Zhou, B. Xiang, Y. Li, G. Li, W. Xiong, Z. Zeng, Epstein-barr virus-encoded circular RNA circBART2.2 promotes immune escape of nasopharyngeal carcinoma by regulating PD-L1, Cancer Res. 81 (19) (2021) 5074–5088, https://doi.org/10.1158/0008-5472.CAN-20-4321.
[81] U. Schnell, V. Cirulli, B.N. Giepmans, EpCAM: structure and function in health and disease, Biochim. Biophys. Acta 1828 (8) (2013) 1989–2001, https://doi.org/10.1016/j.bbamem.2013.04.018.
[82] B. D'souza, J. Taylor-Papadimitriou, Overexpression of ERBB2 in human mammary epithelial cells signals inhibition of transcription of the E-cadherin gene, Proc. Natl. Acad. Sci. U. S. A. 91 (15) (1994) 7202–7206, https://doi.org/10.1073/pnas.91.15.7202.
[83] F.X. Real, W.J. Rettig, P.G. Chesa, M.R. Melamed, L.J. Old, J. Mendelsohn, Expression of epidermal growth factor receptor in human cultured cells and tissues: re-lationship to cell lineage and stage of differentiation, Cancer Res. 46 (9) (1986) 4726–4731. PMID:3015394.
[84] T.M. Bui, H.L. Wiesolek, R. Sumagin, ICAM-1: a master regulator of cellular responses in inflammation, injury resolution, and tumorigenesis, J. Leukoc. Biol. 108 (3) (2020) 787–799, https://doi.org/10.1002/JLB.2MR0220-549R.
[85] F. Kontos, T. Michelakos, T. Kurokawa, A. Sadagopan, J.H. Schwab, C.R. Ferrone, S. Ferrone, B7-H3: an attractive target for antibody-based immunotherapy, Clin. Cancer Res. 27 (5) (2021) 1227–1235, https://doi.org/10.1158/1078-0432.CCR-20-2584.
[86] M.H. Wang, R. Sun, X.M. Zhou, M.Y. Zhang, J.B. Lu, Y. Yang, L.S. Zeng, X.Z. Yang, L. Shi, R.W. Xiao, H.Y. Wang, S.J. Mai, Epithelial cell adhesion molecule overexpression regulates epithelial-mesenchymal transition, stemness and metastasis of nasopharyngeal carcinoma cells via the PTEN/AKT/mTOR pathway, Cell Death Dis. 9 (1) (2018) 2, https://doi.org/10.1038/s41419-017-0013-8.
[87] D. Xiao, M. Xiong, X. Wang, M. Lyu, H. Sun, Y. Cui, C. Chen, Z. Jiang, F. Sun, Regulation of the function and expression of EpCAM, Biomedicines 12 (5) (2024) 1129, https://doi.org/10.3390/biomedicines12051129.
[88] Y. Liu, Y. Wang, S. Sun, Z. Chen, S. Xiang, Z. Ding, Z. Huang, B. Zhang, Understanding the versatile roles and applications of EpCAM in cancers: from bench to bedside, Exp. Hematol. Oncol. 11 (2022) 97, https://doi.org/10.1186/s40164-022-00352-4.
[89] L. Ruan, X.H. Li, X.X. Wan, H. Yi, C. Li, M.Y. Li, P.F. Zhang, G.Q. Zeng, J.Q. Qu, Q. Y. He, J.H. Li, Y. Chen, Z.C. Chen, Z.Q. Xiao, Analysis of EGFR signaling pathway in nasopharyngeal carcinoma cells by quantitative phosphoproteomics, Proteome Sci. 9 (2011) 35, https://doi.org/10.1186/1477-5956-9-35.
[90] C.M. Liu, T.S. Sheen, J.Y. Ko, C.T. Shun, Circulating intercellular adhesion molecule 1 (ICAM-1), E-selectin and vascular cell adhesion molecule 1 (VCAM-1) in head and neck cancer, Br. J. Cancer 79 (2) (1999) 360–362, https://doi.org/10.1038/sj.bjc.6690057.
[91] H. Chen, X. Duan, X. Deng, Y. Huang, X. Zhou, S. Zhang, X. Zhang, P. Liu, C. Yang, G. Liu, Q. Ren, Y. Xiong, B. Zhu, J. Zhang, T. Xiang, EBV-Upregulated B7-H3 inhibits NK cell-mediated antitumor function and contributes to nasopharyngeal carcinoma progression, Cancer Immunol. Res. 11 (6) (2023) 830–846, https://doi.org/10.1158/2326-6066.CIR-22-0374.
[92] J. Yan, Y. Fang, B.J. Huang, Q.W. Liang, Q.L. Wu, Y.X. Zeng, Absence of evidence for HER2 amplification in nasopharyngeal carcinoma, Cancer Genet. Cytogenet. 132 (2) (2002) 116–119, https://doi.org/10.1016/s0165-4608(01)00542-8.
[93] S. Shi, X. Li, B. You, Y. Shan, X. Cao, Y. You, High expression of FGFR4 enhances tumor growth and metastasis in nasopharyngeal carcinoma, J. Cancer 6 (12) (2015) 1245–1254, https://doi.org/10.7150/jca.12825.
[94] A.T. Regua, M. Najjar, H.W. Lo, RET signaling pathway and RET inhibitors in human cancer, Front. Oncol. 12 (2022) 932353, https://doi.org/10.3389/fonc.2022.932353.
[95] E.P. Hui, V.W. Lui, C.S. Wong, B.B. Ma, C.P. Lau, C.S. Cheung, K. Ho, S.H. Cheng, M.H. Ng, A.T. Chan, Preclinical evaluation of sunitinib as single agent or in combination with chemotherapy in nasopharyngeal carcinoma, Invest New Drugs 29 (6) (2011) 1123–1131, https://doi.org/10.1007/s10637-010-9451-1.
[96] Y. Chen, C. Zhou, H. Li, H. Li, Y. Li, Identifying key genes for nasopharyngeal carcinoma by prioritized consensus differentially expressed genes caused by aberrant methylation, J. Cancer 12 (3) (2021) 874–884, https://doi.org/10.7150/jca.49392.